Agriculture - Rice Cultivation Emissions for Modeled and Non-modeled Countries

Authors for Rice Cultivation Emissions for Modeled Countries:
Rudiyanto[1] and Budiman Minasny[2]
1) Universiti Malaysia Terengganu, 2) The University of Sydney

Authors for Rice Cultivation Emissions for Non-Modeled Countries:
Caleb Dittmar[3,4], Lee Gans[3], Rudiyanto[1], Budiman Minasny[2], Sam Schiller[5], Gabriela Volpato[3] and Aaron Davitt[3]
3) WattTime, 4) Williams College, 5) Carbon Yield

The Climate TRACE coalition provides rice cultivation emission estimates using two different methods. First, a remote sensing based approach that estimates emissions for the largest rice producers globally. Second, for countries not modeled, emission factors from the first approach were applied to country data provided by The Food and Agriculture Organization (FAO) FAOSTAT. The remote sensing approach is described here and the methodology discussing non-modeled countries follows. All rice emissions data can be viewed on the Climate TRACE website (https://climatetrace.org/).

Rice Cultivation Emissions for Modeled Countries

1. Introduction

Rice paddy fields play an important role in greenhouse gas emissions as a source of methane (CH_4) emissions. Current estimates of CH_4 emissions from rice cultivation are mostly derived from agricultural statistics (Fung *et al.*, 1991; Li *et al.*, 2002; Yan *et al.*, 2009a; Saunois *et al.*, 2016, 2020; Carlson *et al.*, 2017; Zhang *et al.*, 2020). These reports are usually aggregated to country level and have high-levels of uncertainty. Rice cultivation varies between regions and inaccurate estimates of rice cropping intensities reported in the agricultural statistics can lead to high uncertainty in CH_4 emissions estimates (Zhang *et al.*, 2020).

Satellite-based annual rice cultivation mapping is a spatially resolved method that can improve the estimation of CH_4 emissions from rice paddies. It is supported by results of a recent study by (Zhang *et al.*, 2020) that showed rice cultivation area and cropping intensities derived from Moderate Resolution Imaging Spectroradiometer (MODIS) satellite imagery for monsoon Asian countries (the south, east and southeast Asian countries). The study presents strong spatial

temporal consistencies with atmospheric methane concentration datasets derived from greenhouse gas monitoring satellites, including the Scanning Imaging Absorption Spectrometer for Atmospheric Chartography (SCIAMACHY) on the Environmental Satellite (ENVISAT) and the Thermal and Near Infrared Sensor for Carbon Observation Fourier-Transform Spectrometer (TANSO-FTS) onboard the Greenhouse Gases Observing Satellite (GOSAT).

Here, we employ the Paddy Watch method that uses satellite-data from MODIS measurements to identify global rice fields and associate rice cropping patterns, and apply a CH_4 emissions equation to estimate rice fields emissions. To reflect regional differences in emission factors, this approach employs regional or country-based methane emission factors from rice cultivation.

2. Materials and Methods

Figure 1 shows global rice field areas (Kuenzer and Knauer, 2013). Global rice fields are mainly concentrated in the tropical and sub-tropical regions in Asia (monsoon Asia) which account for 87% of the global paddy rice harvested area and 90% of the rice production (Zhang et al., 2020). Rice fields can also be found in temperate regions in the United States of America (USA; California, Mississippi, Missouri, and Louisiana), Europe (Italy and Spain), and Brazil (Santa Catarina and Rio Grande do Sul). In this study, rice fields and cropping intensity (i.e., single, double or triple rice planting) are mapped for 23 major producing rice countries including India, China, Bangladesh, Indonesia, Thailand, Viet Nam, Myanmar, Philippines, Pakistan, Cambodia, Brazil, Japan, Nepal, USA, Sri Lanka, Lao People's Democratic Republic, Korea (the Republic of), Malaysia, Korea (the Democratic People's Republic of), Iran (Islamic Republic of), Taiwan, Italy and Spain.

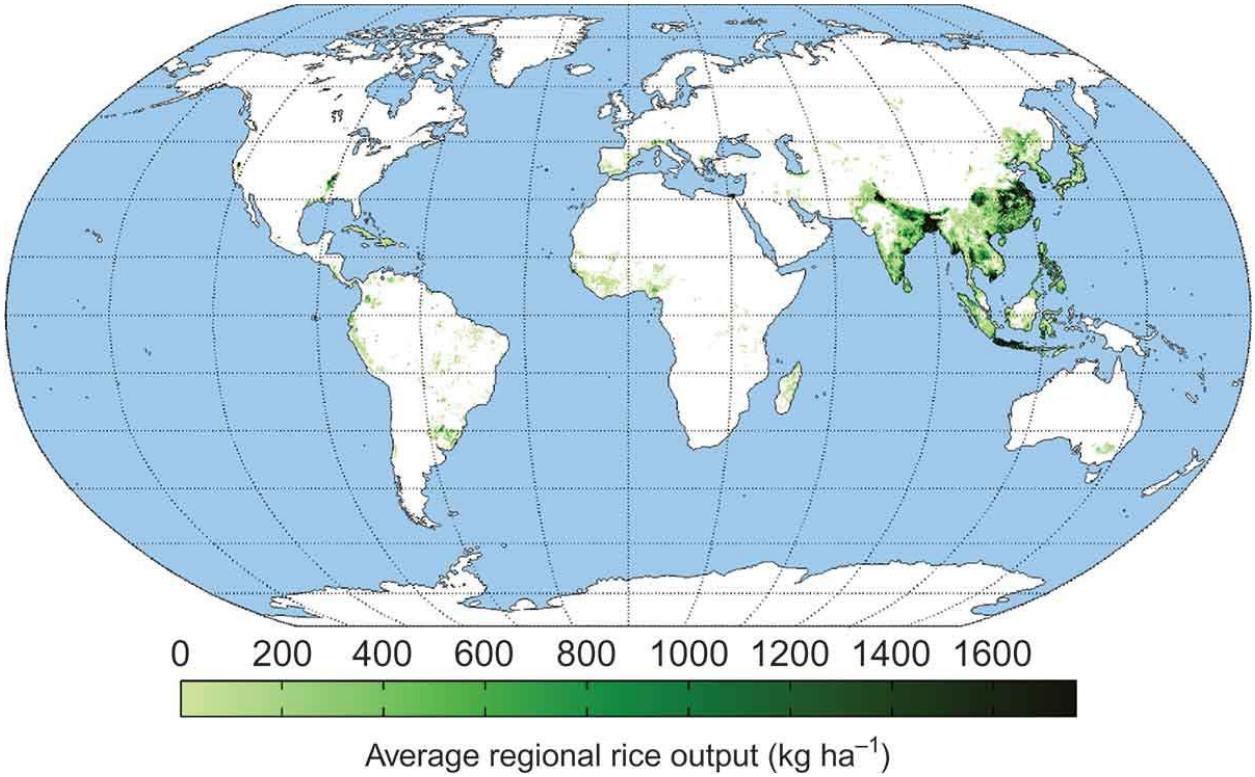

Figure 1 Global paddy rice field areas based on average regional rice output (taken from Kuenzer and Knauer, 2013).

2.1 Datasets employed

2.1.1 Rice emission factors

To reflect regional and national differences in rice emissions, rice emission factors (EFs) were collected from recently published data and summarized in Table S1. This approach was adopted over the IPCC rice EF approach, which can under or overestimate rice methane emissions since a global constant EF is used to estimate emissions. For each major rice production country (see Table S1), either the country-specific EF was used or, if country-specific EF was not available, EFs were used from the respective neighboring countries with similar climates and rice growing conditions.

2.1.2 Remote sensing datasets

For more than two decades, remote sensing technology has been widely used to map rice fields over the world (Dong & Xiao, 2016). Optical, near-infrared (NIR) and shortwave infrared (SWIR) measuring satellites are popular choices for mapping of rice fields in regional and global scales. Specifically, Moderate Resolution Imaging Spectroradiometer (MODIS) data provides excellent temporal resolution and spectral measurements for this effort (Clauss, Yan and Kuenzer, 2016; Gumma *et al.*, 2016; Zhang *et al.*, 2020). MODIS provides red and NIR bands for generating vegetation index that capture rice growth and green and SWIR bands for water

index that can detect the presence of standing water during transplanting and rice phenology or growth stages (Qin *et al.*, 2015; Zhang *et al.*, 2015, 2020; Zhou *et al.*, 2016).

Mapping global rice extent (area) and cropping intensity used the 8-day composite surface reflectance products from MODIS Terra MOD09A1 Version 6 (MOD09A1.006) Surface Reflectance and Aqua MYD09A1 Version 6 (MYD09A1.006) Surface Reflectance, and the Terra and Aqua combined MODIS Land Cover Type (MCD12Q1) Version 6 provides cropland identification based on the land cover scheme of the International Geosphere-Biosphere Programme (IGBP). All products have a native spatial resolution of 500 m. All products were acquired from the Google Earth Engine (GEE) data catalog. Specifications and uses of these datasets are depicted in Table 1.

Table 1 Sources of datasets that are used for estimating harvested rice cultivation extent.

Satellite/Sensor	Bands Employed	Used to	Temporal and Spatial Resolution, and coverage
- MOD09A1.006 Terra Surface Reflectance (MODIS/006/MYD09A1) - MYD09A1.006 Aqua Surface Reflectance (MODIS/006/MOD09A1)	sur_refl_b01 (red) sur_refl_b02 (NIR) sur_refl_b04 (green) sur_refl_b05 (SWIR1) for generating 2 indices: NDVI and NDSI	Identify rice cultivation and cropping intensities	8-day, 500 m, global
MODIS Land Cover Type (MODIS/006/MCD12Q1)	LC_Type1 (the land cover scheme of IGBP)	Mask non-cropland	Annual, 500 m, global

2.1.3 Existing harvested paddy area

To compare harvested rice time series data results generated from this study, two existing datasets were used. First, FAOSTAT paddy rice area harvested in hectares (ha) at the country level from 2000 to 2019 were downloaded (https://www.fao.org/faostat/en/#data/GR). Second, harvested rice area data from 2000 to 2015 in the monsoon Asian countries was extracted from the 500 m spatial resolution paddy rice map of Zhang *et al.* (2020), derived using MODIS data.

2.1.4 Existing inventories of methane emissions from rice cultivation

To compare rice CH_4 emissions generated from this study, FAOSTAT methane emissions (kilotonnes of CH_4) data at the country level were downloaded from FAOSTAT (https://www.fao.org/faostat/en/#data/GR). The FAOSTAT methane emission data were calculated at Tier 1 based on IPCC, 1997 Vol. 3, Ch. 4 and IPCC, 2002. For Asia countries, an area-weighted average EF was used, i.e., 15.7 g $CH_4/m^2/yr$. For all other regions, the IPCC EF

value was set either based on a neighboring country (where one existed), or the IPCC global default EF value (20 g $CH_4/m^2/yr$).

In addition, global methane emission from rice cultivation reported by Saunois *et al.* (2016), Zhang *et al.* (2016) and Carlson *et al.* (2017) were also compared to the results from this study. Note that all three studies used FAOSTAT harvested rice area data as the main source data for their emission estimates.

2.2 Model

CH_4 emissions from rice cultivation strongly depend on the harvested rice extent (IPCC, 1997). To generate methane emissions for this study, a simple approach was used to estimate CH_4 emissions from rice cultivation at region or country-*i* which is given by equation 1 (IPCC, 1997):

$$Emission_i = A_i \text{ x } EF_i \text{ (Eq.1)}$$

$$Total\ Emission = \sum_{i=1}^{N} Emission_i \text{ (Eq.2)}$$

Where *Emission* is the CH_4 emissions (g CH_4 $year^{-1}$), *A* is the rice paddy annual harvested area (m^2) from MODIS-derived indices and *EF* is the emission factor for seasonally rice cultivation (g CH_4 m^{-2} $year^{-1}$) and subscript *i* is for the region or country. To account for paddy rice planting systems (single, 1; double, 2; and triple, 3; see section 2.3.2 for more information), the EF is the emission factor for each rice harvest (thus double and triple cropping systems multiply the appropriate EF by 2 and 3, respectively) to reflect the emissions from these systems. The region based emissions factor for seasonal rice cultivation was determined based on published data and shown in Table S1. To calculate propagation of uncertainty for Eq. 1 and 2, following formula are used, respectively:

$$\Delta Emission_i = A_i \text{ x } \Delta EF_i \text{ (Eq.3)}$$

$$\Delta Total\ Emission = \sqrt{\sum_{i=1}^{N} \left(\Delta Emission_i^2\right)} \text{ (Eq.4)}$$

Where Δ is the standard deviation, given for specific countries and regions in Table S1.

2.3 Methods

Rice area harvested and methane emissions from rice cultivation were processed and generated in the GEE platform with the following steps and shown in Figure 2:

- Collecting MODIS profiles of spectra indices for training data for all countries
- Characterizing and labeling profiles of spectra indices with rice growth stages

- Mapping rice extent, cropping intensity and harvested area from spectra indices
- Aggregating harvested rice area to the country level
- Estimating methane emission using Eq. 1 to 4 in section 2.2

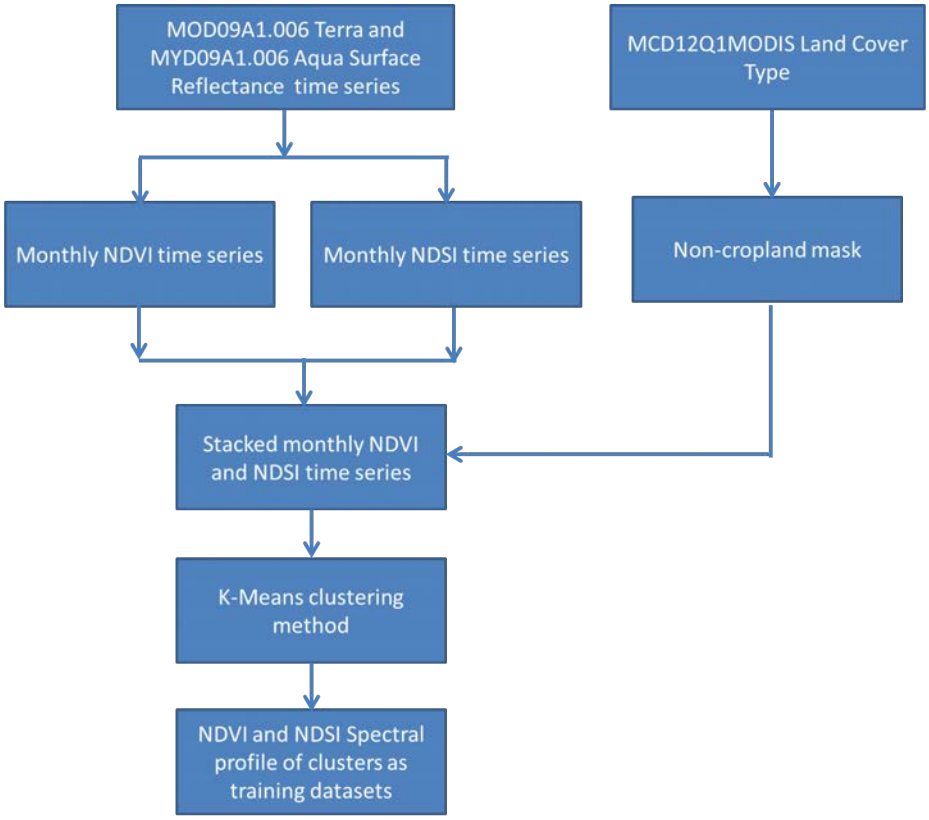

Figure 2 Workflow for collecting profiles of MODIS spectral indices for mapping rice cultivation using the unsupervised K-means method and rice phenology-based approach.

2.3.1 Image processing and collecting profiles of spectral indices for training data

MOD09A1.006 Terra Surface Reflectance and MYD09A1.006 Aqua Surface Reflectance were used to generate monthly time series of maximum composites for two spectral indices: the Normalized Difference Vegetation Index, NDVI (Eq.5) and Normalized Difference Snow Index, NDSI (Eq. 6):

$$NDVI = (NIR - RED)/(NIR + RED) \text{ (Eq. 5)}$$

$$NDSI = (GREEN - SWIR)/(GREEN + SWIR) \text{ (Eq. 6)}$$

Note that NDSI is not only useful to identify snow, but also the presence of water/flooding. Thus, it is also known as Modified Normalized Difference Water Index (MNDWI) and that the NDSI formula is also referred to as the Normalized Difference Water Index (NDWI; McFeeters, 1996; Xu, 2006). The monthly NDVI composites are the maximum monthly value taken for each

month for NDVI and subsequently used to calculate the monthly NDSI composites. The monthly NDVI composites are used to minimize the effect of clouds, since the NDVI value of rice fields is larger than the NDVI of clouds (Fatchurrachman *et al.*, 2022).

Figure 3a, b and c show rice field images in very high resolution imagery from Google Earth, MODIS NDVI and NDSI, respectively. MODIS NDVI and NDSI images show that rice fields have a different tone compared to other land cover types. Moreover, rice fields, built-up, tree and water bodies also can be differentiated from NDVI and NDSI time series data as shown in Figure 4. Note that both indices show spectral time series profiles of the double rice crop which has two peaks of rice growth season. Meanwhile, the built-up, tree and water body values are relatively constant at 0.2, 0.8 and -0.1, respectively, for NDVI and -0.3, -0.8 and 0.1, respectively, for NDSI. NDVI and NDSI time series imagery data were used to determine the uniqueness of rice fields in a phenology based method and described in section 2.3.2.

For each country modeled, a year of time series monthly maximum composites NDVI and NDSI spectral indices were stacked that resulted in 24 bands of images. After that, to create a rice cultivation map, the non-croplands in the region of interest were masked using the MODIS MOD12Q1 land cover map. Masking out non-cropland areas also reduced computational memory and time. To identify rice class in the stacked images, an unsupervised K-Means clustering method was employed in GEE. The K-Means algorithm normalizes the numerical inputs and measures distances between clusters using the Euclidean distance, and then iteratively modifies the centroids (cluster means) for minimizing distance or variation of within-cluster variation (Rudiyanto *et al.*, 2019). The K-Means was used due to its ability to generalize clusters from the data pattern and can learn from the data and cluster time series data into unique spectral responses related to rice phenology or other land uses (see Figure 3). Additionally, this algorithm identifies reflectance signatures due to soil tillage and planting, as well as vegetative, reproductive, and maturity stages (see Section 2.3.2). Nevertheless, prior knowledge is still required to identify the reflectance signature. Figure 3d and e presents the illustration of the cluster and grouping results of rice extent. Subsequently, the centroid of each cluster was determined and then used to produce monthly time series of NDVI and NDSI spectral profiles. The workflow is shown in Figure 2.

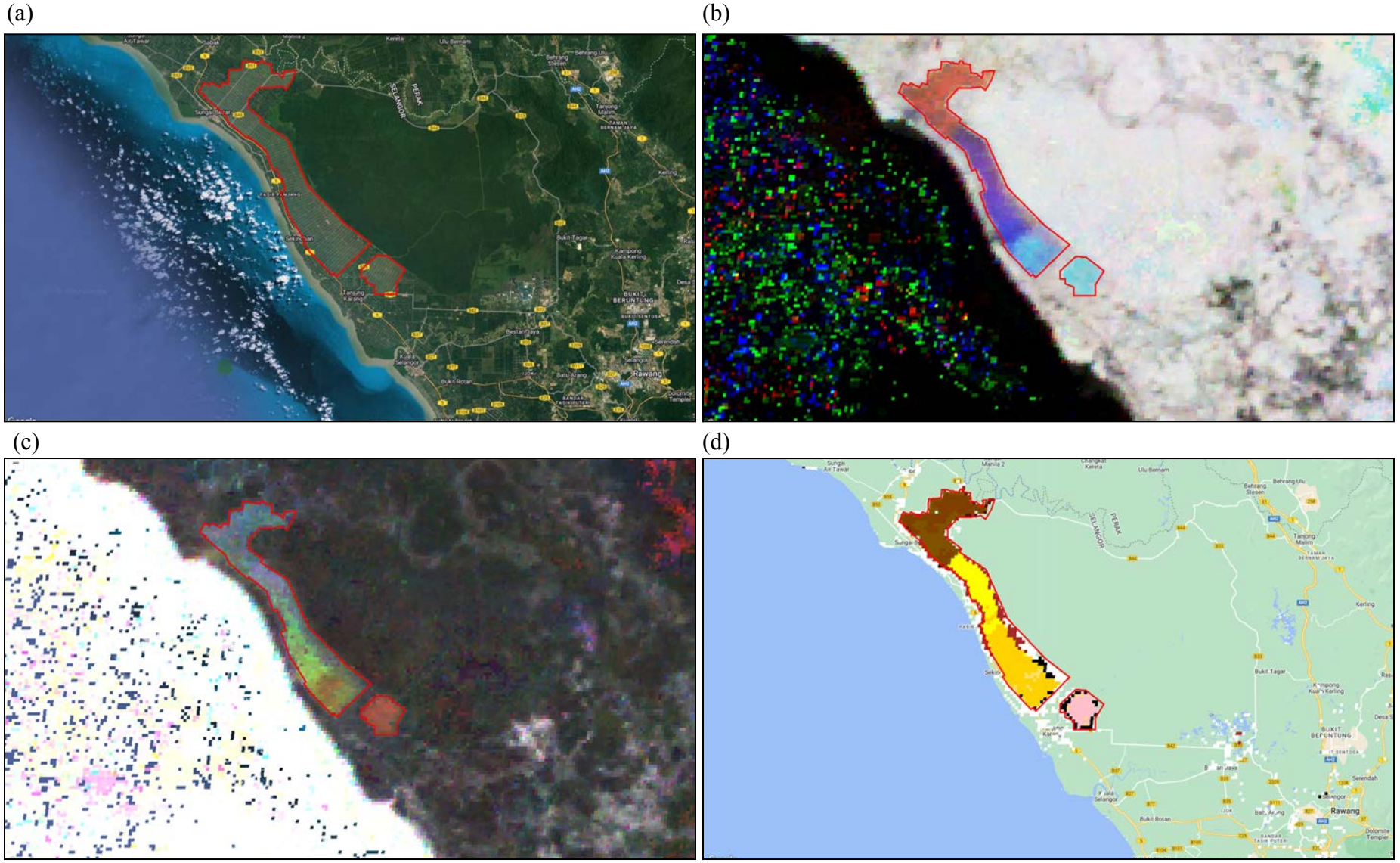

Figure 3 cont.

(e)

Figure 3 Rice field imagery shown in (a) Very High Resolution Imagery (VHRI) from Google Earth, (b) MODIS NDVI and (c) MODIS NDSI images acquired for year 2021, (d) cluster results and (e) grouping of rice field clusters (green pixels) in Selangor, Malaysia (coordinates: 101.107ºE, 3.551ºN). NDVI and NDSI are false colors with January, February and March 2021 images as red, green and blue channels, respectively.

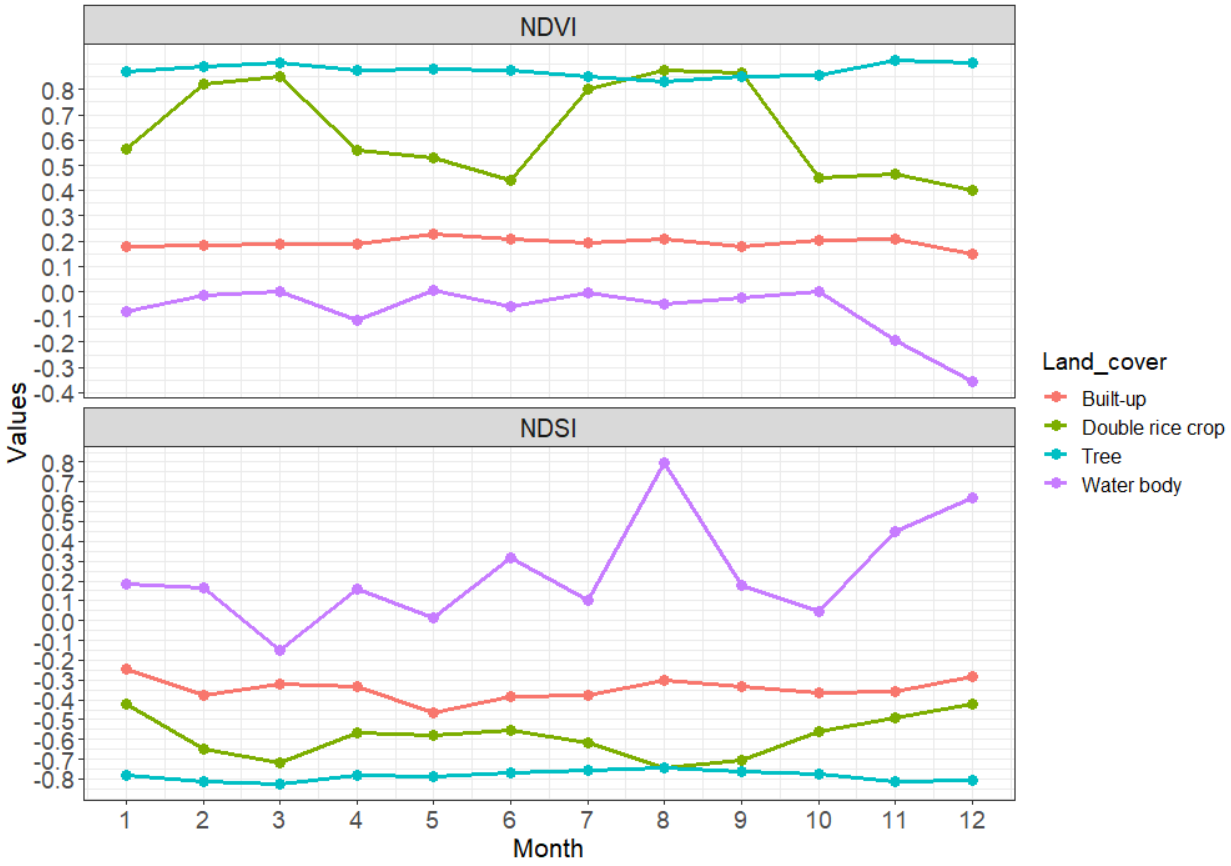

Figure 4 Temporal profile signature of NDVI (top) and NDSI (bottom) for different types of land cover types- double rice crop (green line), built-up (red line), tree and (light blue line) water body (purple line) at Selangor, Malaysia.

2.3.2 Characterizing spectral indices of rice phenology

Rice phenology generally can be divided into three stages (1) tillage and transplanting (30 days after planting), (2) growth stages including: vegetative (30-45 days after tillage), generative (30 days after vegetative) and (3) maturity (30 days after generative) (Sianturi, Jetten and Sartohadi, 2018; Rudiyanto *et al.*, 2019). The full rice growing cycle can take 4-5 months depending on the varietal. Based on rice phenology, the response of the NDVI and NDSI spectra to three key phenological periods, as shown in Figure 5, can be described as follows (Rudiyanto *et al.*, 2019; Zhang *et al.*, 2020; Fatchurrachman *et al.*, 2022):

(a) The tillage and transplanting (T) period, where rice fields are irrigated. During this period, a peak in the NDSI profile can be identified which indicates the presence of standing water in the rice field. Figure 5 demonstrates that the peak could be detected in May (month 5) in the NDSI profile by visual inspection. The range values of this peak vary depending on locations.

(b) The growth stages: vegetative (V) and generative (G) period, where rice grows rapidly with canopy closure. As a result, chlorophyll contents increase significantly. During this period, NDVI values rapidly increase and peak at the end of the generative period, when

the crop enters the heading or maturity stage (NDVI values were larger than 0.7). Figure 5 displays this peak between June and July (months 6 and 7).

(c) The maturity (M) period, where chlorophyll content rapidly decreases, as the carotenoid content increases. During this period, NDVI values drop distinctly, indicating the maturity of the rice plant. This period occurs in the last month of the rice growth cycle, after August (month 8; Figure 5).

These three spectral characteristics can be used to differentiate rice fields from other land covers (Rudiyanto *et al.*, 2019; Zhang *et al.*, 2020; Fatchurrachman *et al.*, 2022).

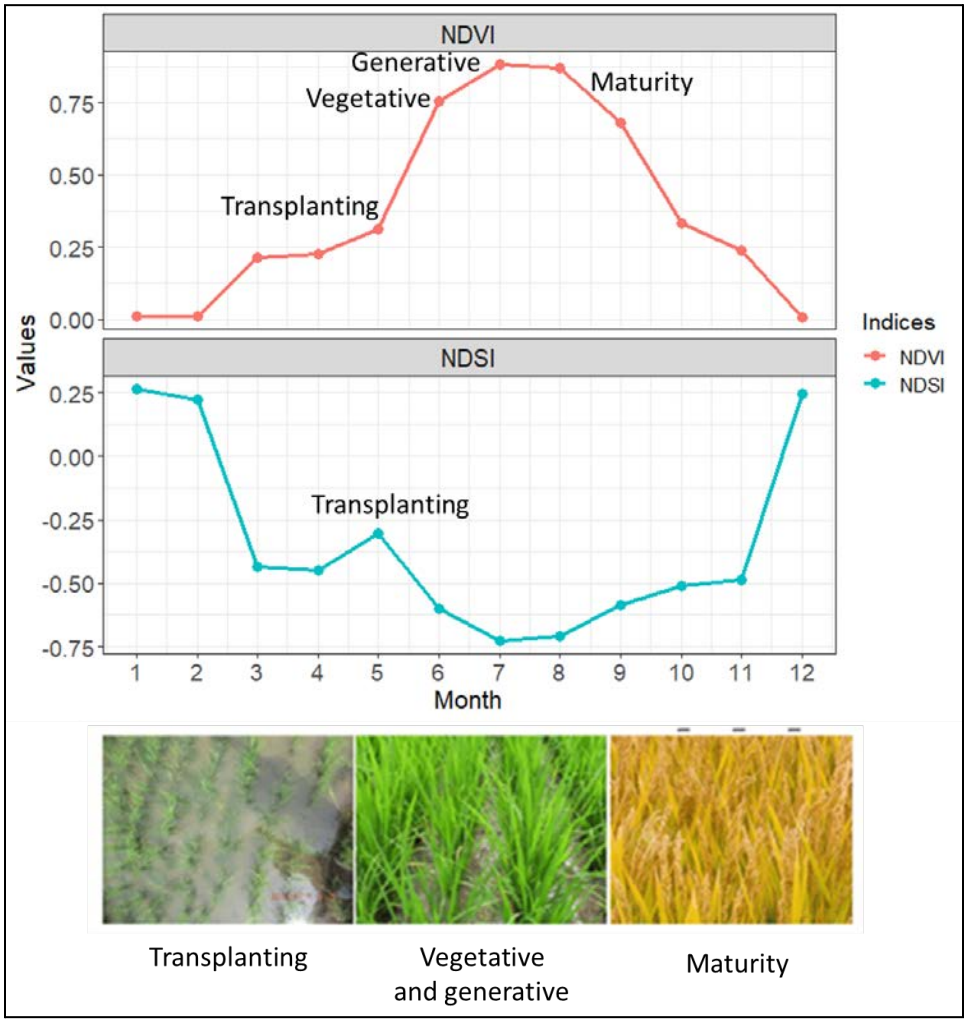

Figure 5 Temporal responses of NDVI (top) and NDSI (bottom) profiles to three phenology stages of rice growth comprising: (1) tillage and transplanting in May; (2) growth stages: vegetative and generative in June and July and (3) maturity in August at Heilongjiang region, China. The images are from (Dong and Xiao, 2016).

Temporal NDVI and NDSI profiles were also used to identify paddy rice system intensity. Paddy rice intensity and its area were used to estimate the annual harvested paddy rice area and

subsequently used to calculate annual methane emissions from rice cultivation (See Eq. 1). Figure 6 shows the standard NDVI and NDSI temporal profile for different paddy rice planting systems (single, double, and triple) on Java Island, Indonesia. Since rice fields are distributed in different climatic zones from tropical to temperate regions, the temporal NDVI and NDSI profiles were acquired for every country and the process was conducted at the country-level. Thus, this phenology-based algorithm is very useful for mapping rice area and cropping intensities across climatic zones (Dong and Xiao, 2016).

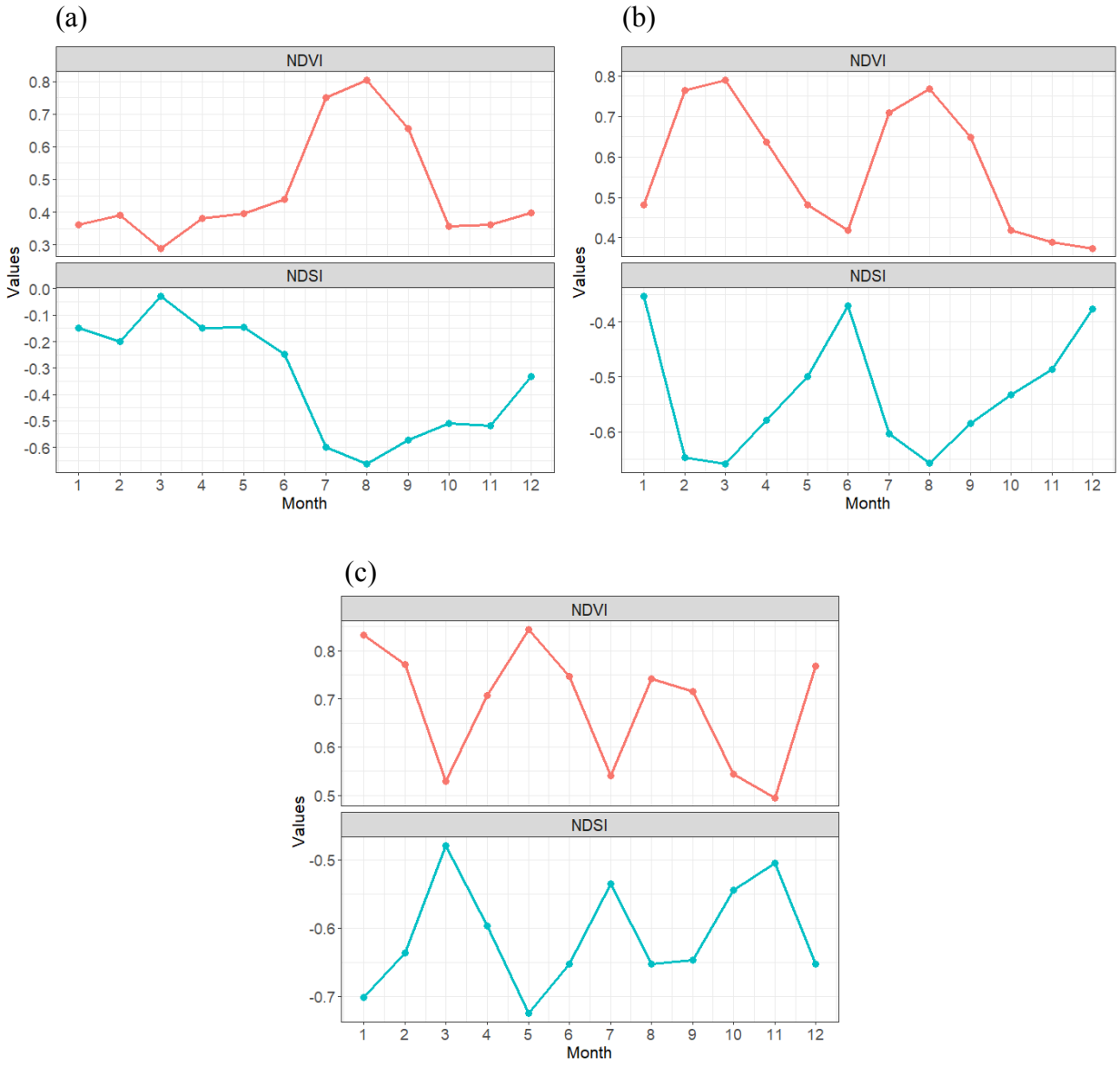

Figure 6 Temporal profile analysis of NDVI and NDSI for three different types of (a) single, (b) double and (c) triple paddy rice at Java island, Indonesia.

2.3.3 Automated mapping of rice extent and cropping intensity

Identified and labeled temporal NDVI and NDSI rice profiles were used as a training dataset for mapping rice area harvested in other countries. The minimum distance method with Euclidean

distance in GEE was used as a classifier to automatically classify and map rice extent and intensity. The minimum distance method uses the mean vectors of each endmember and calculates the Euclidean distance from each unknown pixel to the mean vector for each class. All pixels are classified to the nearest class. Figure 7 shows the workflow of mapping rice intensity and the annual area harvested of rice.

2.3.4 Identifying rice cultivation and estimating annual methane emissions

Once the annual rice area harvested was determined, annual methane emissions from rice cultivation was calculated using Eq. 1. Zonal statistics was employed to compute annual rice area harvested and methane emissions from rice cultivation on cell values of a raster (a value raster) within the country level. In these zonal statistics, the zones are specified as the grouping cropping intensity and the statistic is determined by the reducer sum to get the total area of the single, double and triple cropping system.

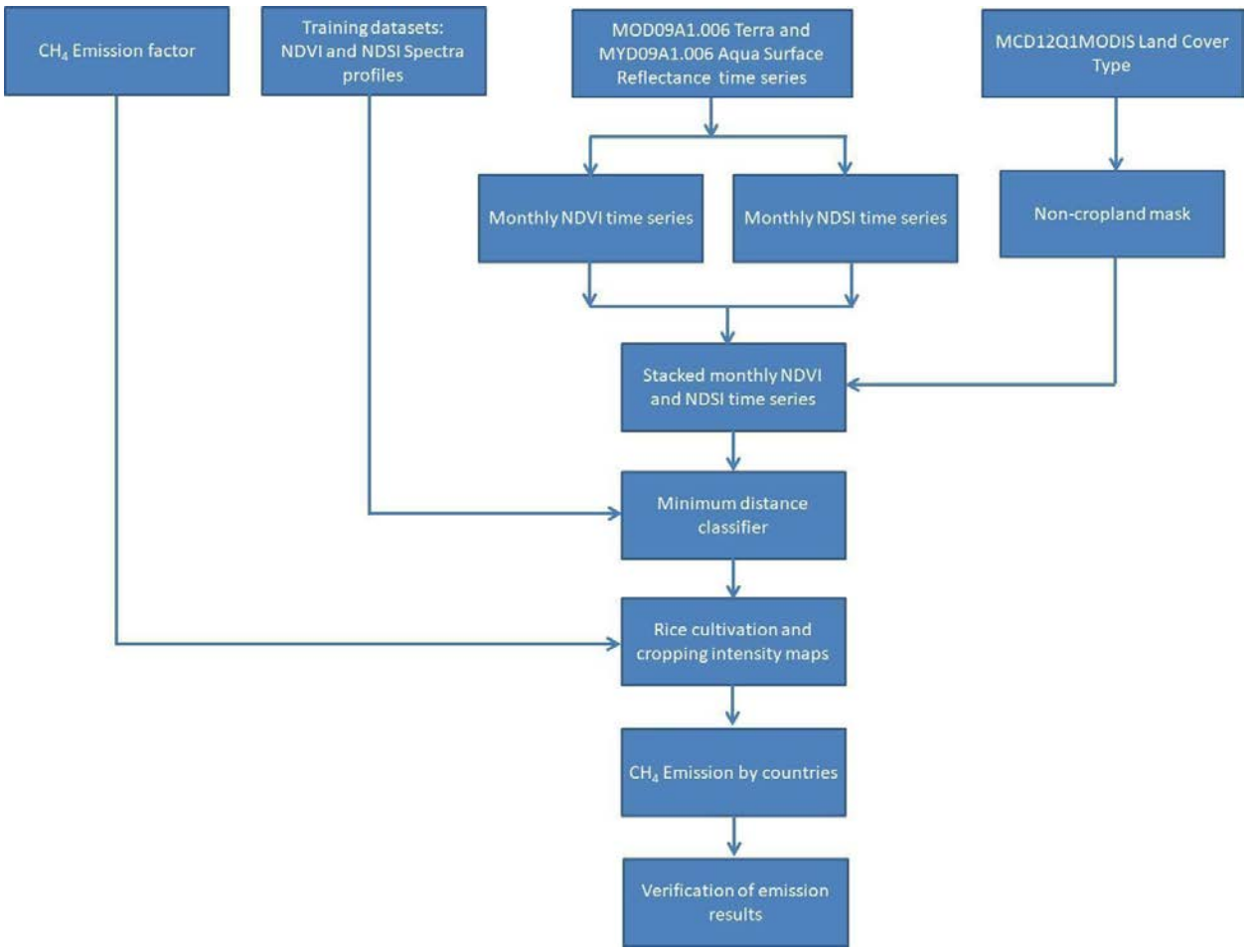

Figure 7 Workflow for mapping rice area harvested and estimating CH_4 emissions from rice cultivation using satellite-based annual rice cultivation map.

2.4 Verifying modeled emissions estimates

Annual rice area harvested and methane emission from rice cultivation were compared to FAOSTAT data**.** In addition, annual rice area harvested data were also compared with the data from paddy rice map from Zhang *et al.* (2020). See section 2.1.2 and 2.1.3 for details on each dataset.

3. Results

3.1 Annual spatial-temporal rice area harvested

Spatial distribution of rice extent and intensity for 23 major producing rice countries are estimated for years 2015 to 2021. An example of this is shown in Figure 8a, b and c for Southeast Asian, East Asian and South Asian countries, respectively. From the rice intensity, the single rice crop was dominant and can be found especially in temperate regions like China, India, Korea and Japan and in dry regions like Thailand, Myanmar and Cambodia. For double rice crops, it is distributed especially in the Southeast Asian countries like Indonesia, Viet Nam, Malaysia and Philippines. Triple rice crop area was smallest and can be found only at Mekong delta, Viet Nam and East Java, Indonesia.

(a) Southeast Asian countries

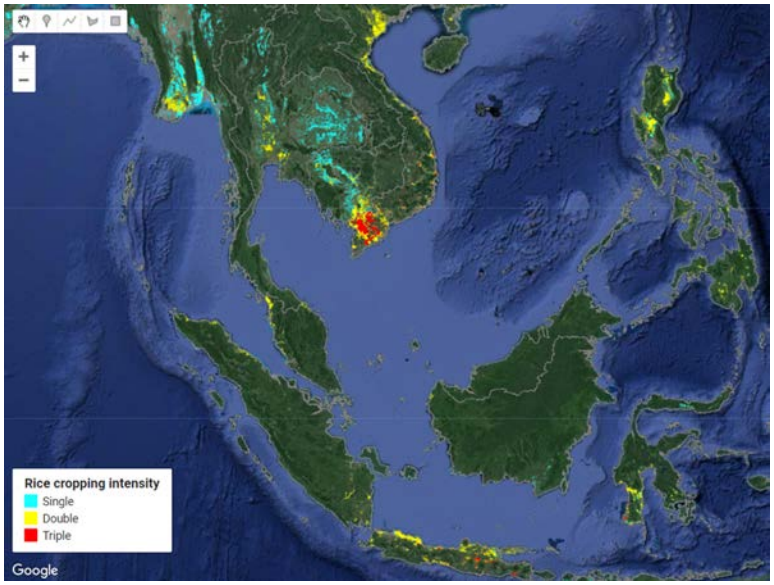

(b) East Asian countries

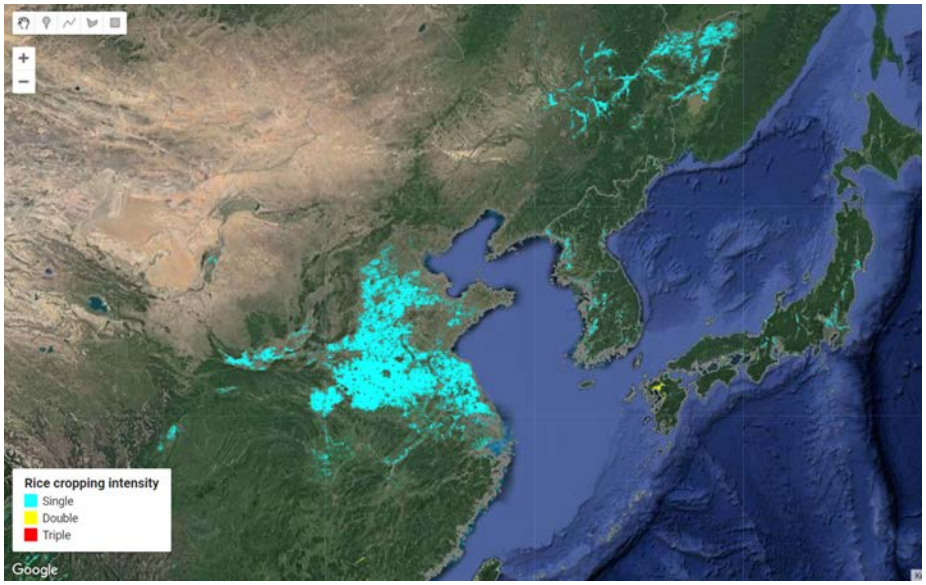

(c) South Asian and north parts of Southeast Asian countries

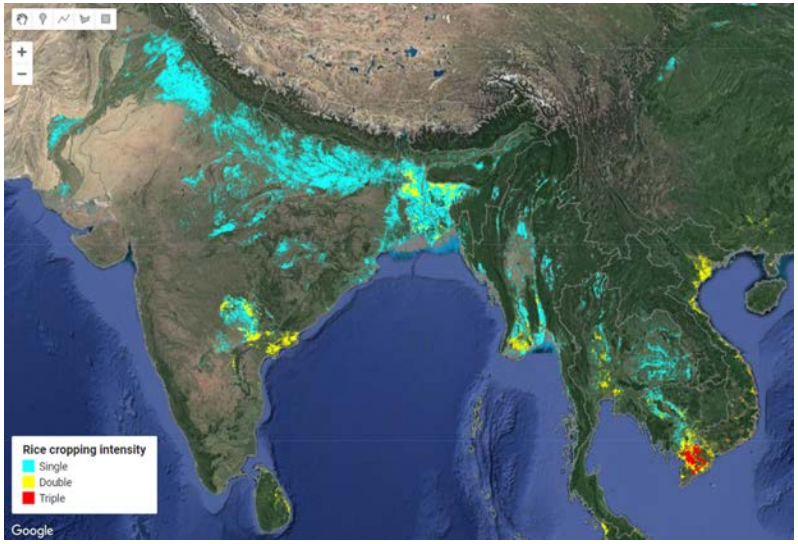

Figure 8 Spatial distribution of rice cultivation extent and intensity for the year 2021 in (a) Southeast Asian, (b) East Asian and (c) South Asian countries derived from Paddy Watch using MODIS data. Light blue, yellow and red color are for single, double and triple rice intensity crops, respectively. Apps for rice intensity extent for the year 2021 are available as follows:
https://rudiyanto.users.earthengine.app/view/harvestedpaddy

(a) 23 countries

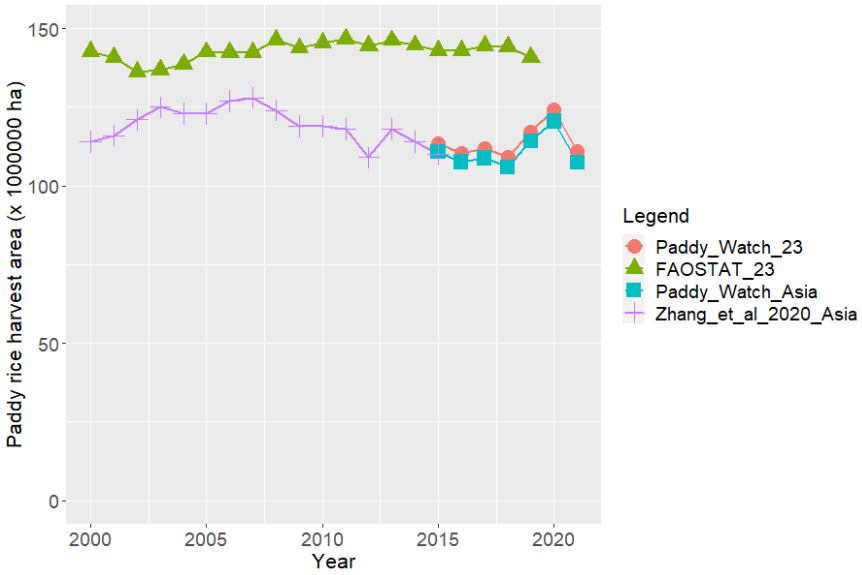

(b) India

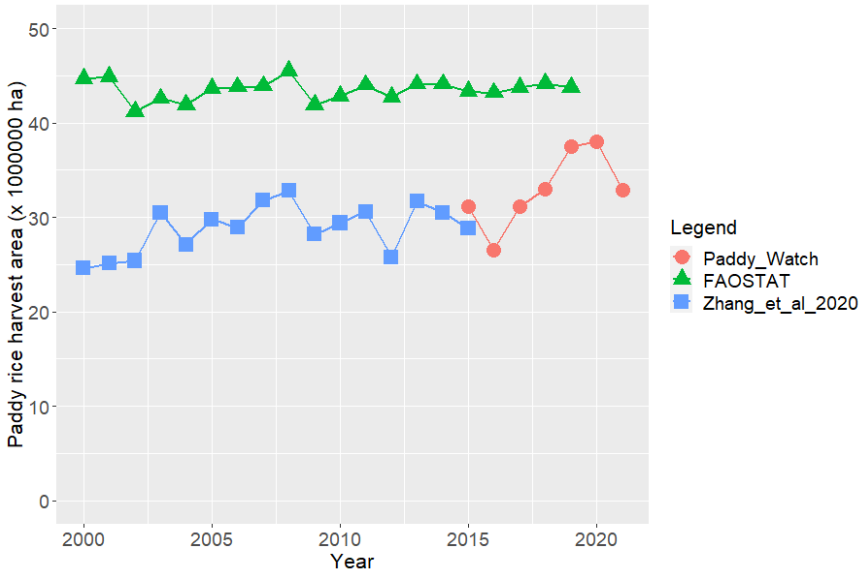

(c) China

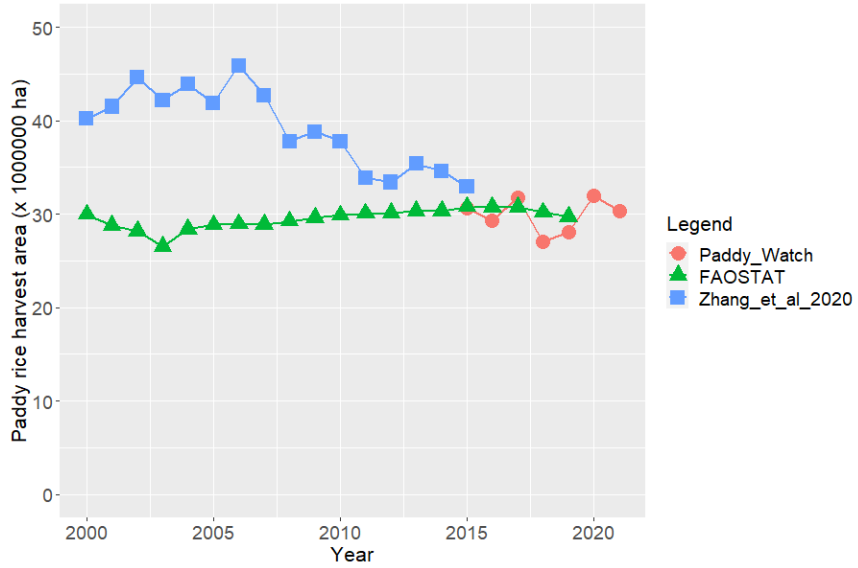

Figure 9 Annual paddy rice area harvested based on Paddy watch (2015 - 2021), FAOSTAT data (2000 - 2019) and Zhang *et al.* (2020) (2000 - 2015) for (a) 23 countries and Asian monsoon countries, (b) India and (c) China.

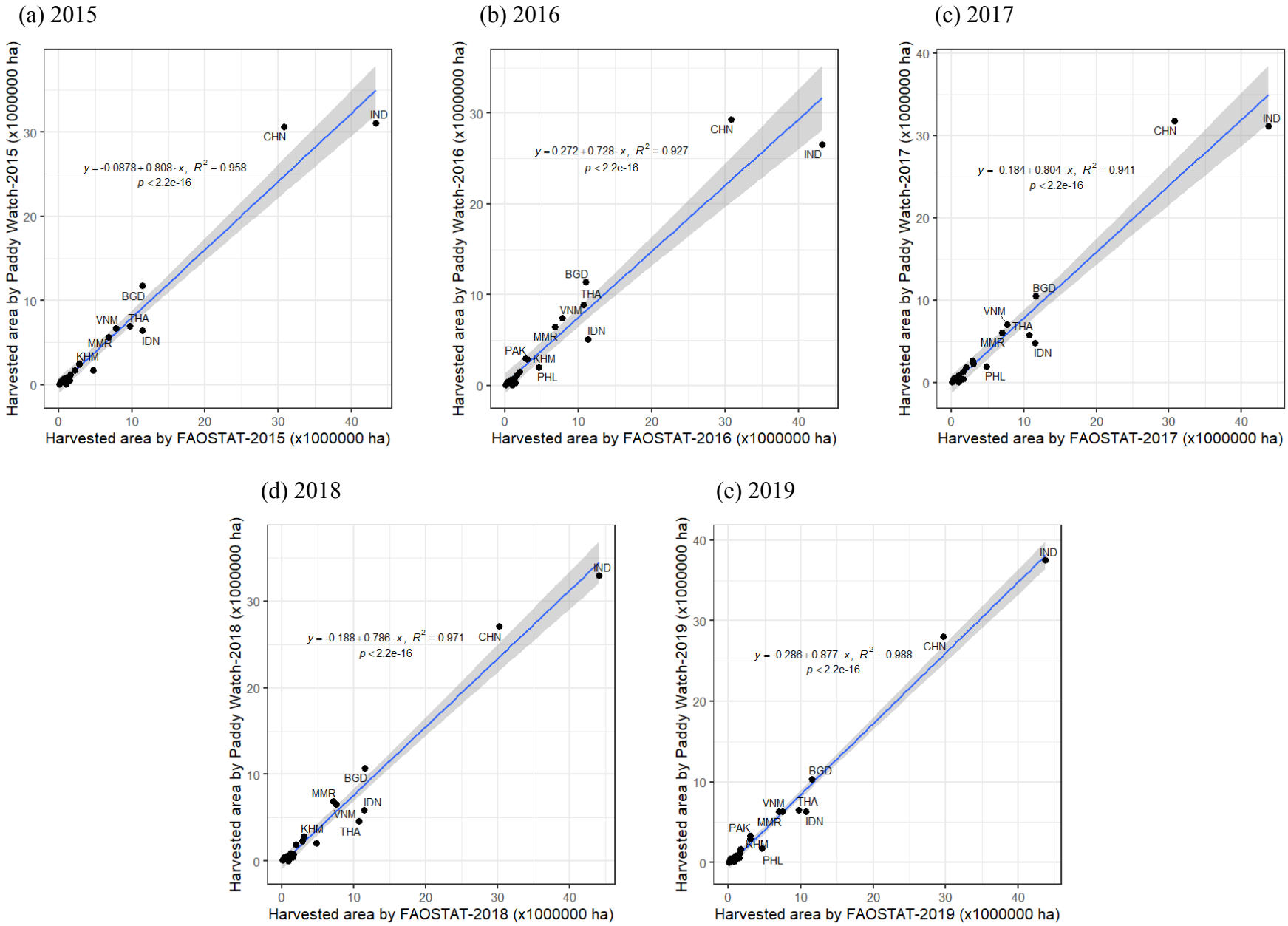

Figure 10 Correlation analysis of annual harvested area between Paddy watch and FAOSTAT data for 2015 to 2019. Shaded area represents the 95% confidence interval.

Annual rice area harvested data from this study was compared to FAOSTAT and paddy rice extent from Zhang *et al.* (2020) and shown in Figure 9a, while the Paddy Watch results for the 23 countries are presented in Table S2. By comparison, the data from this study (available for 2015-2021) and Zhang *et al.* (2020) (available 2010-2015), derived from the same MODIS data, have overlapping data in 2015 with average values of 114 and 119 million ha, respectively. Both rice areas harvested data from this study and Zhang *et al.* (2020) also have similar ranges, 109 to 124 million ha and 109 to 128 million ha, respectively. Meanwhile, FAOSTAT data from 2010 to 2019 show larger harvested values relative to the two remote sensing derived data, with a relatively constant value of 143 million ha and a range between 136 and 147 million ha. Additionally, Paddy Watch data continues the lower time series trend observed in Zhang *et al.* (2020) relative to the FAOSTAT reported data.

Figure 9b and c shows annual rice harvested for the two largest rice producing countries in terms of rice area harvested: India and China. For India, the dataset from this study and (Zhang *et al.*, 2020) overlapped and showed an increasing trend of rice paddy area harvested from 25 million ha in the year of 2000 into 37 million ha in 2020, with a decrease to 33 million ha in 2021. Again, FAOSTAT data shows significantly larger values than this study and (Zhang *et al.*, 2020). The FAOSTAT rice area harvested data for 2000 - 2019 varies between 40 and 45 million ha.

For China, the Paddy Watch data and (Zhang *et al.*, 2020) show overlap in 2015 with a value of 111 million ha and the Paddy Watch data continues the observed decreasing trend of rice paddy area harvested observed in Zhang *et al.* (2020)- from 45 in 2006 into 30 million ha in 2020. Opposite of India, FAOSTAT data shows lower values for rice area harvested in China (Zhang *et al.*, 2020), reporting fairly consistent annual values of ~30 million ha from 2008 to 2019.

Figure 10 shows the correlation between harvested rice cultivation from Paddy Watch and FAOSTAT for 2015 to 2019. No comparison is available for FAOSTAT-2020 and 2021 due to the time lag with compiling information. There are strong positive linear relationships between Paddy Watch and FAOSTAT data with $R^2 > 0.9$. From 2015 to 2019, Figure 10 also shows that FAOSTAT reported larger annual harvested paddy area than Paddy Watch in some countries like India (IND), Thailand (THA), Indonesia (IDN) and Philippines (PHL). Meanwhile, the annual harvested paddy area in China (CHN), Viet Nam (VNM) and Bangladesh (BGD) reported by FAOSTAT agreed well with Paddy Watch results.

3.2 Annual spatial-temporal methane emissions

Region based rice emission factors (Table S1) were used to determine rice methane emissions from 2015 to 2021 using Eq (1) and the results are listed in Table S3. The resulting map at 500 m resolution of annual CH_4 emission estimates from rice cultivation in Southeast Asian, East Asian and South Asian countries for the year 2021 are shown in Figure 11a, b and c, respectively. The

largest emissions are mainly found in rice cultivation at the Mekong delta region, Viet Nam; Java island, Indonesia and Kyushu island, Japan that have two and three rice cropping systems.

Figure 12a shows the temporal variation of summed annual methane emissions from rice cultivation in 23 major producing rice countries that derived from this study (available from 2015 to 2021) and FAOSTAT data (available from 2015 to 2019). It should be noted that the methane emission data for 2020 and 2021 are still unavailable from FAOSTAT at the time of this study. The methane emission from rice cultivation in this study is lower than FAOSTAT data for all years. The 2015 to 2021 mean value for Paddy Watch data from this study was 20 million tonnes CH_4 while the 2015 to 2019 mean value for FAOSTAT data was 23.8 million tonnes CH_4. The methane emission from rice cultivation ranges between 18.9 to 21.6 million tonnes for Paddy Watch data during 2015 to 2021 and 23.4 to 24.0 million tonnes for FAOSTAT data during 2015 to 2019.

For India and China, temporal variation of annual methane emission from this study and FAOSTAT data are presented in Figure 12b and c, respectively. For whole years, it shows that China methane emissions from this study (7.5 million tonnes CH_4) are higher than the data in FAOSTAT data (5.3 million tonnes CH_4), while methane emissions for India in this study (2.7 million tonnes CH_4) are lower than FAOSTAT data (4.6 million tonnes CH_4). However, China's rice harvested area displays the opposite results, where Paddy Watch estimates are lower than FAOSTAT values. This indicates that the differences are mainly due to the emission factors employed here in this study. The FAOSTAT emission factors used for China (175.63 kg/ha/season) was lower than this study's value (249.4 kg/ha/season). Similarly, the FAOSTAT emission factor used for India (105.56 kg/ha/season) was larger than this study's emission factor (81 kg/ha/season).

Figure 13 shows the correlation between annual methane emission from 23 countries based on Paddy Watch and FAOSTAT for 2015 to 2019. Similar to correlation analysis for annual harvested paddy rice area, strong linear relationships were found between Paddy Watch and FAOSTAT with R^2 ranging 0.74 to 0.81. As with China, Paddy Watch estimates indicate higher rice emissions for Brazil (BRA), Japan (JPN), Bangladesh (BGD) and Viet Nam (VNM) for years 2015 to 2019. Similar to India (IND), Indonesia (INA), Philippines (PHL), Thailand (THA) and Myanmar (MYR), Paddy Watch estimates indicate lower rice emissions for 2015 to 2019.

(a) Southeast Asian countries

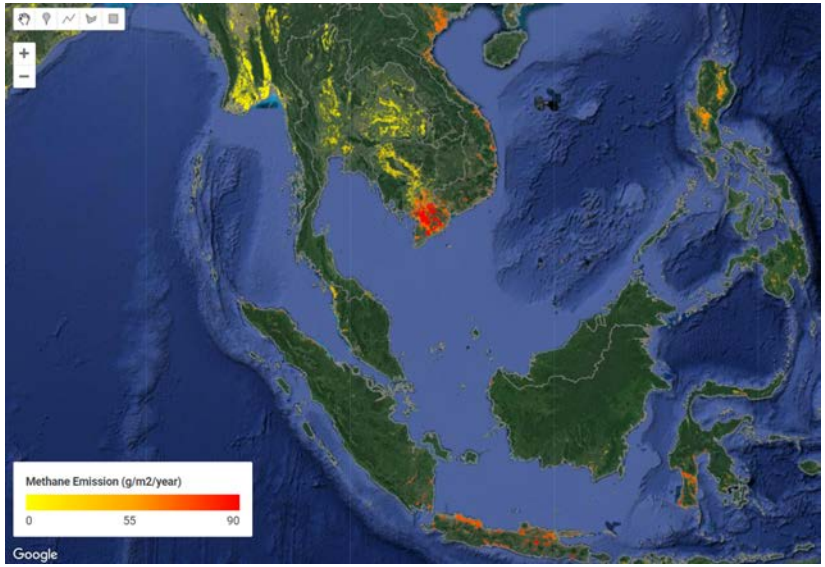

(b) East Asian countries

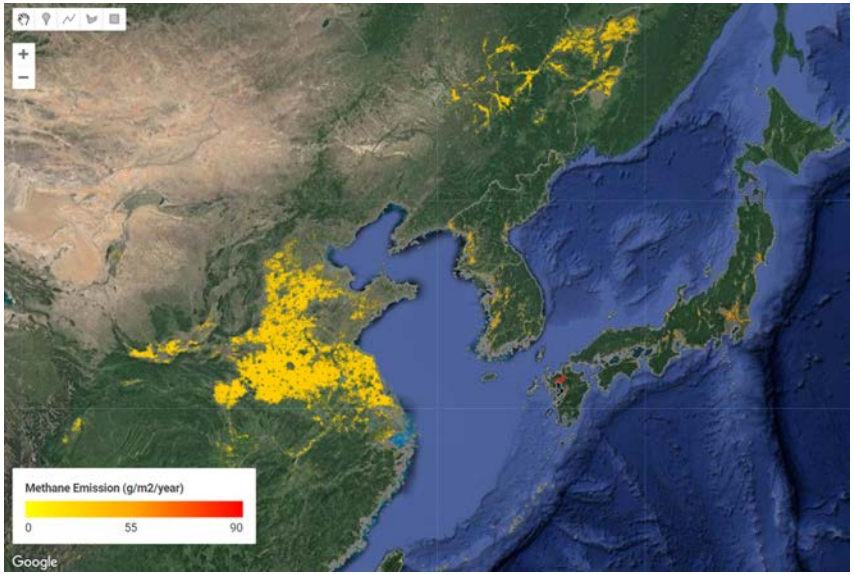

(c) South Asian and north parts of Southeast Asian countries

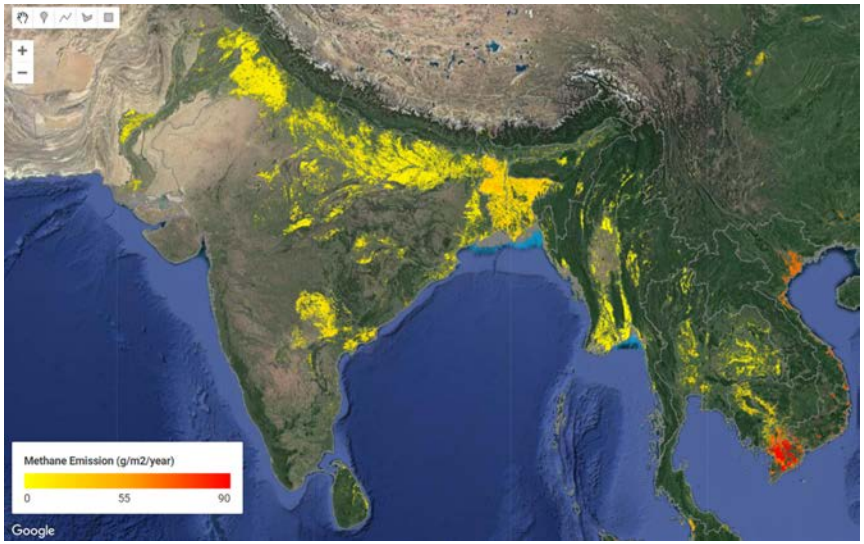

Figure 11 Spatial distribution of annual CH_4 emission estimates for the year 2021 from rice cultivation in (a) Southeast Asian, (b) East Asian and (c) South Asian countries derived from Paddy Watch using Eq. (1). Apps for rice intensity extent for the year 2021 are available as follows: https://rudiyanto.users.earthengine.app/view/paddymethane

(a) 23 countries

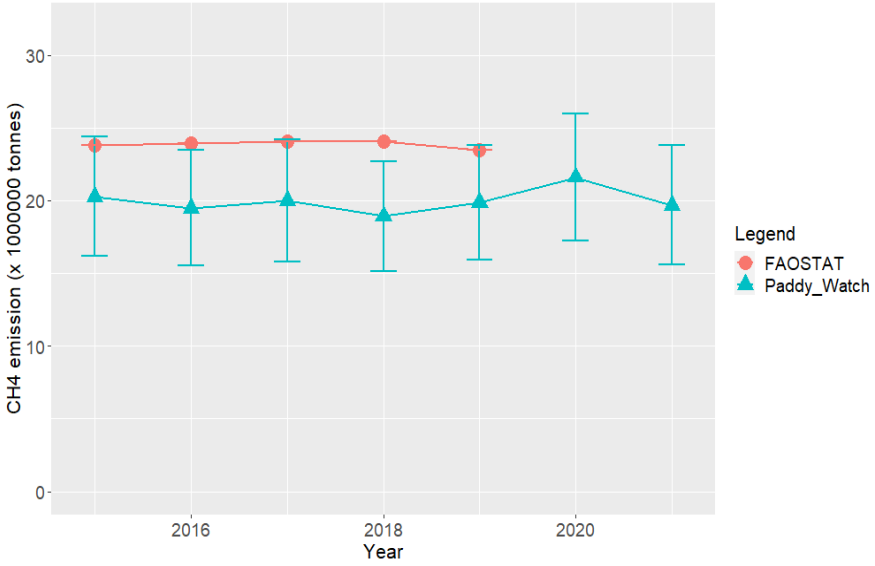

(b) India

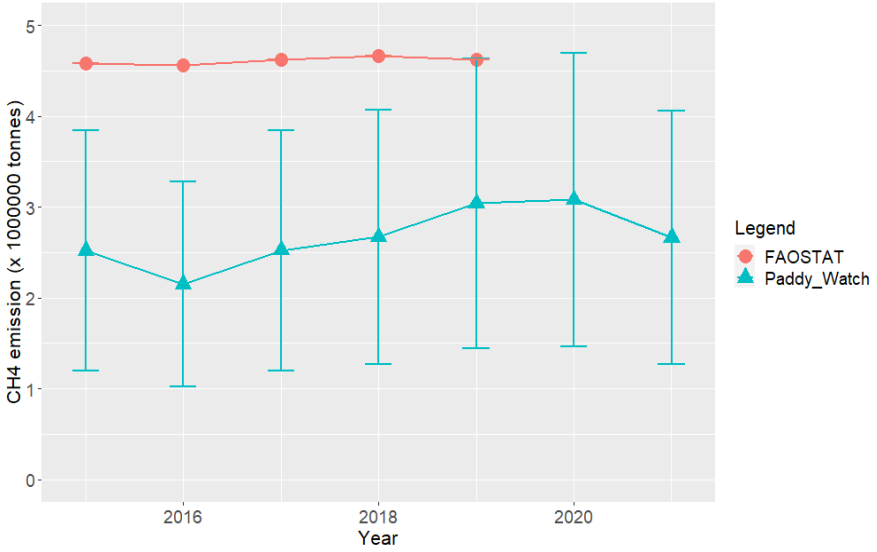

(c) China

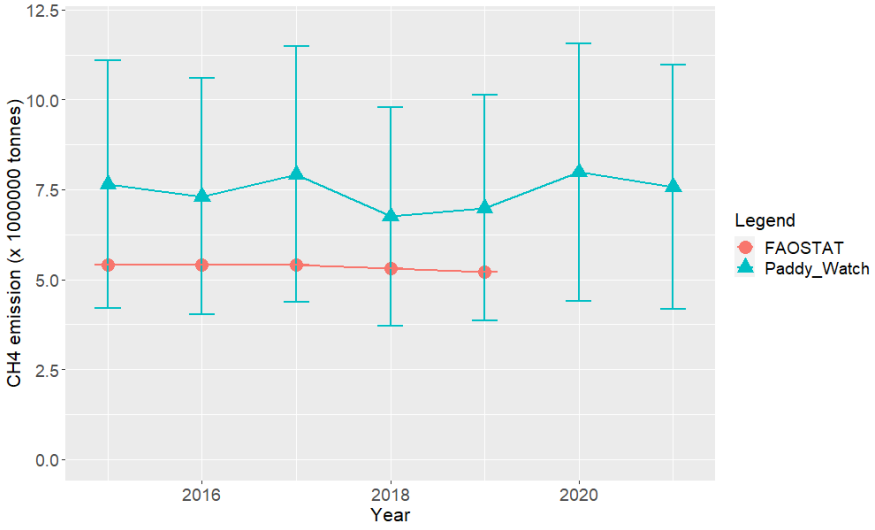

Figure 12 Annual methane emission from rice cultivation based on Paddy watch, FAOSTAT data and Zhang *et al.* (2020) for (a) 23 countries, (b) India and (c) China. Vertical light blue bars represent standard deviation.

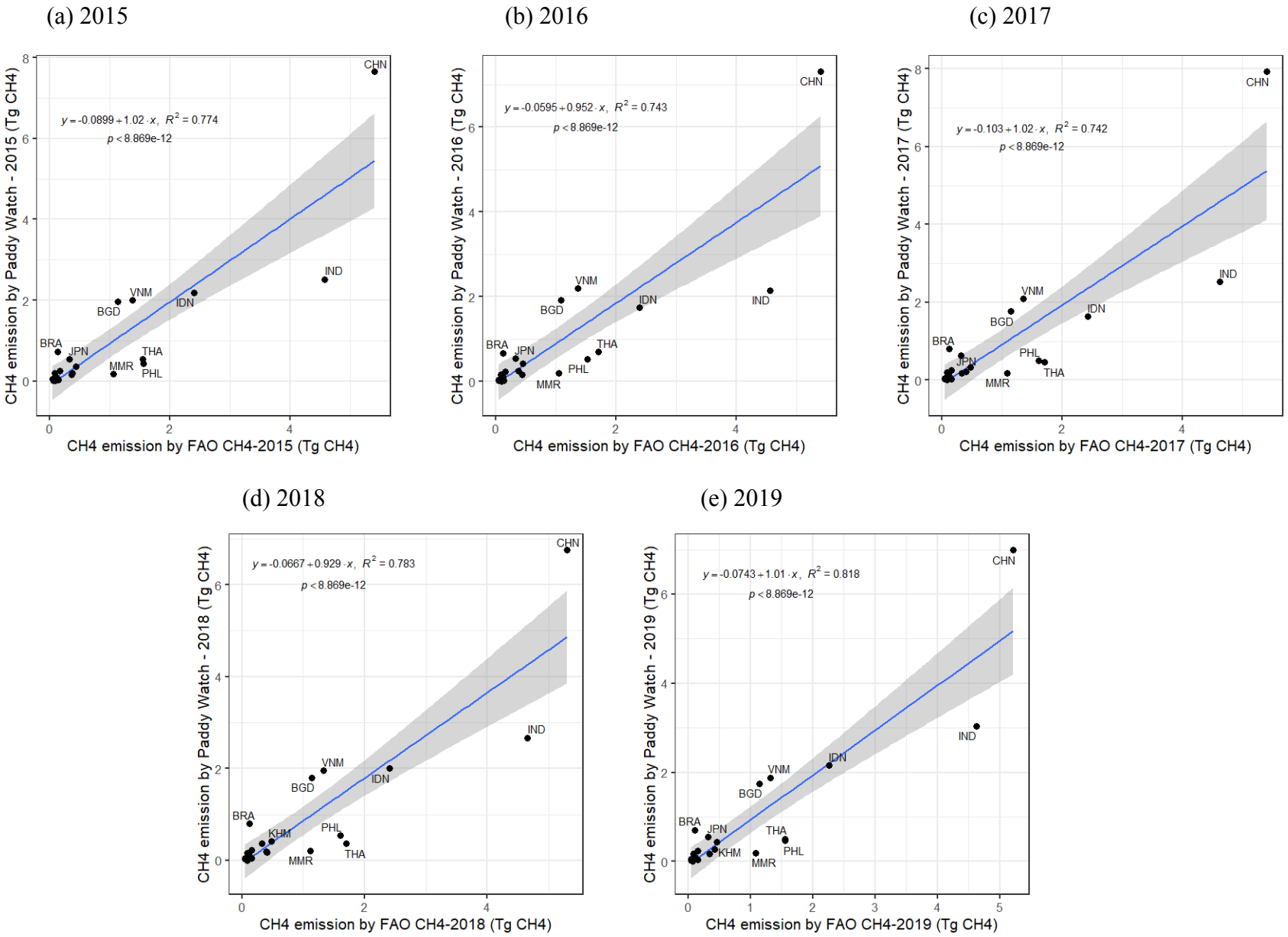

Figure 13 Correlation analysis of annual methane emission from rice cultivation between Paddy watch and FAOSTAT data for 2015 to 2019. Shaded areas represent the 95% confidence interval.

To understand if significant changes in global CH_4 emission from rice cultivation has occurred, the Paddy Watch emissions estimates are also compared to other rice emission inventories in Table 2. Most studies use FAOSTAT harvested rice area, while emission factor values vary based on empirical studies and process-based modeling - commonly IPCC 2006 Guidelines emission factors are applied. To account for the scaling factor which represents rice water regime such as irrigated and rainfed rice areas, Zhang *et al.* (2016) and Carlson *et al.* (2017) use the MIRCA2000—Global monthly irrigated and rainfed crop areas around the year 2000 (Portmann, Siebert and Döll, 2010). For the CH_4 emission estimates based on process-based modeling, Zhang *et al.*2016) use the Dynamic Land Ecosystem Model version 2.0 (DLEM v2.0; Tian *et al.*, 2015) for simulating spatiotemporal variation of CH_4 emissions from global rice fields with various scenarios accounting multiple environmental factors in agricultural management practices such as irrigation, nitrogen fertilizer use, and rotation etc. Our global estimate of CH_4 emission from rice cultivation was for the year 2020, while previous studies were for 2000 to 2019.

Table 2 presents 2019, 2020 and 2021 CH_4 estimation for rice cultivation from 23 major rice-producing countries were 19.85, 21.6 and 19.7 Tg CH_4, respectively. The Paddy Watch values are slightly lower than the previous years' estimates from other studies. We note that this estimate assumes a constant emission factor with time and does not consider temporal variability in climate, soil, and management.

Table 2 Estimates of total annual global methane emission from rice cultivation using various inventory approaches. Units are in Terra grams (Tg).

Harvested rice area data (source included)	Year	Total global methane emission (Tg CH_4/year)	Emission factor
Paddy Watch (23 major producing rice countries)	2019 2020 2021	19.85 ± 3.93 21.60 ± 4.35 19.7 ± 4.11	Region based emission factor in Table S1
FAOSTAT-2019 for 23 major producing rice countries (FAO-CH_4; http://www.fao.org/faostat/en/#data/GR; accessed 25 June 2021)	2019	24.08	Emission factor based on IPCC seasonal emission including the scaling factors for rice paddy water regime and a correction factor for organic amendments
Census data from FAOSTAT, Monthly irrigated and rainfed rice areas MIRCA2000 (Zhang *et al.*, 2016)	2000	20.45 (18.3–38.8)	Emission estimates based on process-based modeling
FAOSTAT (Saunois *et al.*, 2020)	2017	30 (24–40)	- FAO-CH_4 (database accessed in February 2019, FAO, 2019) - EDGARv4.3.2 was extrapolated to 2017 using the extended FAO-CH_4 emissions - USEPA (2012)
FAO's AQUASTAT database or FAOSTAT and MIRCA2000 (Carlson *et al.*, 2017)	2000	28.3	IPCC emission and scaling factors

4. Discussion

The inventory approach is commonly used to estimate global CH_4 emissions from rice cultivation. The inventory method estimates CH_4 emissions from rice cultivation based on harvested rice area (usually taken from FAOSTAT) from country-specific statistical data, emission factors, and scaling and correction factors (IPCC, 1997). This approach relies on a country's report that lacks spatial detail, can be years out of date and can contain errors, such as under and overreporting rice area cultivated. This can result in emission estimates that are years out of date.

This study is the first to apply harvested rice cultivation derived from MODIS data using the Paddy Watch method. Moreover, the Paddy Watch method uses region based emission factors to

estimate methane emission from rice cultivation. Additionally, this method is implemented in the Google Earth Engine platform and has many advantages, including the creation of harvested rice cultivation data that can be provided rapidly and objectively. The Paddy Watch approach can reduce uncertainty as it identifies where rice was planted, grown and harvested. In addition, the use of region based emission factors can consider spatial variability of climate, soil and management factors that influence methane emission from rice cultivation.

Differences in harvested rice cultivation area between self-reported statistical data and remote-sensing estimates could be a result of measurement error from either source. With regard to remote-sensing estimates, the moderate spatial resolution (500m) of MODIS data can create mixed pixels in which rice and non-rice fields are combined. This could lead to rice area overestimates, especially in lowland regions (Frolking *et al.*, 1999; Seto, Kaufmann and Woodcock, 2000). With regard to self-reported statistics, agricultural data is typically collected in the context of allocating and evaluating agricultural subsidies. The structure of subsidies programs can create incentives to over- or under-report the area of planted rice fields (Yamashita, 2009; Gale, 2013). Because the administration of these programs varies between countries, this could create country-specific biases in the accuracy of self-reported data.

Other factors that contribute to the discrepancy in CH_4 emission between inventories are different emission and scale factors related to water regime and organic amendment. These values can lead to high uncertainty since the availability of these data are limited and quite variable. To reduce this uncertainty, we employ region-based emission factors from previously published data (See Table S1). Uncertainty of methane emission from rice cultivation were also accounted for in this study, which was not accounted for in the previous studies shown in Table 2.

5. Conclusion

Here, we successfully applied MODIS-derived data to identify harvested rice cultivation areas to estimate global CH_4 emission for years 2015 - 2021. This approach was applied to the 23 major rice producing countries, representing 73% of the global rice area for the years 2015-2021 (based on FAOSTAT-2019 data). From these countries, the estimated global CH_4 emissions from rice cultivation for the following years were:

- 20.27 ± 4.11 Tg CH_4 for 2015,
- 19.49 ± 3.96 Tg CH_4 for 2016,
- 20.01 ± 4.20 Tg CH_4 for 2017,
- 18.92 ± 3.77 Tg CH_4 for 2018,
- 19.85 ± 3.93 Tg CH_4 for 2019,
- 21.60 ± 4.35 Tg CH_4 for 2020 and
- $19.722.2 \pm 4.11$ Tg CH_4 for 2021.

At the time of this study, it should be noted that the 2020 and 2021 estimates were still not available in any national self-reporting.

The application of the Paddy Watch approach for deriving the spatially-resolved global harvested rice cultivation area will help provide updated rice emissions data in a timely fashion. Including region-based emission factors and quantifying uncertainty, makes the study more relevant to local conditions and reflects the range of uncertainty of rice emissions monitoring relative to previously produced studies and inventory methodologies. As a next step to refine the estimation of CH_4 rice emissions, finer spatial resolution data will be employed from the Sentinel-1A/B Synthetic Aperture Radar (SAR) and Sentinel-2A/B multispectral satellites, as was done by Fatchurrachman *et al.* (2022). These two satellites provide measurements at 10 meter spatial resolution, capable of identifying smaller rice areas which can better capture the harvested area. Currently, this approach has been applied to Southeast Asia and emissions data from this approach is being incorporated into the Climate TRACE website (https://climatetrace.org/). This will be an improvement over the coarser 500 meter MODIS data employed here. In addition, supporting data related to emission factors and scaling such as water regime and organic amendment are required in order to improve and reduce uncertainty in rice emission estimates for the future.

6. Supplementary materials

Table S1 Seasonally integrated methane emission factors in various conditions and locations of the world that were used in this study. Mean emission factors and standard deviation (SD) are provided.

Country	ISO3 country	Mean CH_4 Emission (kg CH_4/ha/season)	SD CH_4 Emission (kg CH_4/ha/season)	References
Bangladesh	BGD	168.2	80.4	(Islam *et al.*, 2020)
Brazil	BRA	430.1	149.6	(Camargo *et al.*, 2018; Zschornack *et al.*, 2018)
China	CHN	249.4	112.1	(Wang *et al.*, 2021)
Spain	ESP	405.7	202.9	(Moreno-García, Guillén and Quílez, 2020; Martínez-Eixarch *et al.*, 2021)
Indonesia	IDN	339.8	102.1	(Setyanto *et al.*, 2018)
India	IND	81.0	42.5	(Bhatia *et al.*, 2005; Kritee *et al.*, 2018; Oo *et al.*, 2018)
Iran (Islamic Republic of)	IRN	81.0	42.5	India EF
Italy	ITA	292.0	116.0	(Lagomarsino *et al.*, 2016; Mazza *et al.*, 2016; Meijide *et al.*, 2017)
Japan	JPN	469.8	302.4	(Camargo *et al.*, 2018; Toma *et al.*, 2019)
Cambodia	KHM	145.3	31.0	(Vibol and Towprayoon, 2010)
Korea (the Republic of)	KOR	349.4	93.0	(Gutierrez, Kim and Kim, 2013; Lim *et al.*, 2021)
Lao People's Democratic Republic (the)	LAO	78.3	31.6	Thailand EF
Sri Lanka	LKA	81.0	42.5	India EF

Myanmar	MMR	30.1	12.5	(Win *et al.*, 2020)
Malaysia	MYS	178.3	118.5	(Fazli and Man, 2014)
Nepal	NPL	81.0	42.5	India EF
Pakistan	PAK	81.0	42.5	India EF
Philippines (the)	PHL	258.0	192.7	(Alberto *et al.*, 2014; Sander, Samson and Buresh, 2014; Sibayan *et al.*, 2018)
Korea (the Democratic People's Republic of)	PRK	349.4	93.0	Korea (the Republic of) EF
Thailand	THA	78.3	31.6	(Maneepitak *et al.*, 2019)
Taiwan (Province of China)	TWN	112.0	91.4	(Chang, 2001)
United States of America (the)	USA	202.0	121.9	(Hatala *et al.*, 2012; Humphreys *et al.*, 2019; Della Lunga *et al.*, 2021; Karki *et al.*, 2021)
Viet Nam	VNM	296.4	192.9	(Vo *et al.*, 2020)

Table S2 Paddy Watch estimated harvested rice area from 2015 to 2021.

Country	Total harvested rice area (ha)						
	2015	**2016**	**2017**	**2018**	**2019**	**2020**	**2021**
Bangladesh	11,722,099	11,390,790	10,494,788	10,706,153	10,354,925	10,533,907	9,919,869
Brazil	1,705,117	1,552,095	1,862,587	1,858,515	1,647,357	2,451,437	2,272,437
China	30,668,234	29,297,656	31,775,354	27,069,813	28,016,761	32,011,764	30,341,048
Spain	57,073	66,740	60,865	70,270	57,416	65,273	42,658
Indonesia	6,418,245	5,115,649	4,807,663	5,884,907	6,333,339	5,940,978	5,049,681
India	31,099,433	26,547,064	31,142,254	32,948,990	37,507,779	37,998,818	32,839,797
Iran (Islamic Republic of)	438,720	459,006	481,011	443,787	475,010	480,013	452,676
Italy	249,798	246,889	272,184	223,495	228,346	255,077	254,488
Japan	1,152,732	1,142,066	1,354,468	774,127	1,166,029	1,417,582	787,003
Cambodia	2,477,348	2,865,851	2,258,524	2,796,305	2,973,638	3,206,400	2,822,447
Korea (the Republic of)	725,939	637,299	731,611	646,772	663,891	582,734	506,503
Lao People's Democratic Republic (the)	83,059	84,822	58,403	50,484	73,054	106,813	73,750
Sri Lanka	415,282	505,872	295,592	450,945	423,805	462,413	423,349
Myanmar	5,660,412	6,454,030	6,025,846	6,862,234	6,284,441	6,109,520	6,449,182
Malaysia	528,699	555,024	555,646	533,263	528,144	563,571	534,847
Nepal	503,739	333,358	404,065	460,038	582,118	358,420	240,570
Pakistan	2,426,216	2,972,961	2,686,320	2,266,149	3,264,274	3,200,601	2,424,602
Philippines (the)	1,716,010	2,036,777	1,918,415	2,087,605	1,792,274	2,231,418	2,191,635
Korea (the Democratic People's Republic of)	571,608	458,883	542,728	433,129	482,753	429,052	386,799
Thailand	6,968,991	8,904,965	5,823,496	4,583,288	6,525,230	7,603,941	4,264,336
Taiwan (Province of China)	393,349	404,458	435,282	406,908	449,544	416,666	330,992
United States of America (the)	805,662	809,288	842,400	828,627	845,675	970,727	817,421
Viet Nam	6,730,065	7,418,882	7,032,186	6,587,277	6,348,753	6,872,247	7,513,935
Total	***113,517,830***	***110,260,425***	***111,861,688***	***108,973,081***	***117,024,556***	***124,269,372***	***110,940,025***

Table S3 Rice methane emissions for the 23 countries modeled for 2015 to 2021, based on harvested area in Table S2 and emission factors in Table S1. Total and standard deviation (SD) are provided for each country per year.

Country	CH_4 Emission (tonnes CH_4/year)													
	2015		2016		2017		2018		2019		2020		2021	
	Total	SD	Total	SD	Total	SD	Total	SD	Total	SD	Total	SD	Total	SD
Bangladesh	1,972,097	942,810	1,916,358	916,162	1,765,617	844,097	1,801,176	861,097	1,742,087	832,848	1,772,198	847,243	1,668,894	797,856
Brazil	733,371	255,114	667,556	232,219	801,099	278,674	799,347	278,065	708,528	246,472	1,054,363	366,776	977,375	339,994
China	7,648,495	3,436,429	7,306,680	3,282,853	7,924,604	3,560,483	6,751,068	3,033,219	6,987,231	3,139,326	7,983,564	3,586,973	7,566,896	3,399,767
Spain	23,152	11,578	27,073	13,539	24,690	12,348	28,505	14,256	23,291	11,648	26,478	13,242	17,304	8,654
Indonesia	2,181,134	655,270	1,738,468	522,282	1,633,804	490,838	1,999,888	600,819	2,152,280	646,602	2,018,942	606,543	1,716,050	515,547
India	2,520,091	1,321,216	2,151,197	1,127,815	2,523,561	1,323,035	2,669,966	1,399,792	3,039,380	1,593,466	3,079,171	1,614,327	2,661,118	1,395,153
Iran (Islamic Republic of)	35,551	18,638	37,195	19,500	38,978	20,435	35,962	18,854	38,492	20,180	38,897	20,393	36,682	19,231
Italy	72,941	28,968	72,092	28,631	79,478	31,564	65,261	25,918	66,677	26,480	74,482	29,580	74,310	29,512
Japan	541,496	348,568	536,486	345,343	636,261	409,570	363,646	234,084	547,742	352,589	665,909	428,655	369,695	237,977
Cambodia	360,059	76,864	416,524	88,918	328,255	70,075	406,417	86,760	432,190	92,262	466,020	99,484	410,216	87,571
Korea (the Republic of)	253,664	67,518	222,690	59,274	255,646	68,046	226,001	60,155	231,982	61,747	203,624	54,199	176,987	47,109
Lao People's Democratic Republic (the)	6,501	2,628	6,639	2,684	4,571	1,848	3,951	1,597	5,718	2,312	8,360	3,380	5,772	2,334

Sri Lanka	33,652	17,643	40,992	21,491	23,953	12,558	36,542	19,158	34,342	18,005	37,471	19,645	34,305	17,985
Myanmar	170,378	70,671	194,266	80,579	181,378	75,233	206,553	85,675	189,162	78,462	183,897	76,278	194,120	80,518
Malaysia	94,267	62,642	98,961	65,761	99,072	65,835	95,081	63,183	94,168	62,576	100,485	66,774	95,363	63,371
Nepal	40,820	21,401	27,013	14,162	32,743	17,166	37,278	19,544	47,171	24,730	29,044	15,227	19,494	10,220
Pakistan	196,604	103,074	240,909	126,302	217,681	114,125	183,634	96,274	264,515	138,678	259,355	135,973	196,474	103,006
Philippines (the)	442,788	330,724	525,556	392,545	495,015	369,734	538,672	402,341	462,466	345,423	575,780	430,058	565,515	422,391
Korea (the Democratic People's Republic of)	199,736	53,164	160,347	42,680	189,645	50,478	151,348	40,285	168,688	44,900	149,923	39,905	135,159	35,976
Thailand	545,457	220,515	696,984	281,774	455,800	184,269	358,730	145,026	510,725	206,474	595,154	240,607	333,766	134,934
Taiwan (Province of China)	44,073	35,954	45,318	36,970	48,771	39,787	45,592	37,193	50,369	41,091	46,686	38,085	37,086	30,254
United States of America (the)	162,744	98,215	163,476	98,657	170,165	102,694	167,383	101,015	170,826	103,093	196,087	118,338	165,119	99,649
Viet Nam	1,994,496	1,298,263	2,198,631	1,431,139	2,084,032	1,356,543	1,952,180	1,270,718	1,881,492	1,224,706	2,036,633	1,325,690	2,226,801	1,449,475
Total	***20,273,565***		***19,491,412***		***20,014,818***		***18,924,179***		***19,849,523***		***21,602,523***		***19,684,502***	

Rice Cultivation Emissions for Non-modeled Countries

1. Introduction

The following methodology estimates methane emissions from rice production using regional emissions factors and nationally reported harvested rice area estimates, for countries where spatial delineation of rice paddies have not yet been independently modeled. Climate TRACE member Universiti Malaysia Terengganu modeled rice cultivation emissions for 23 major rice producing countries globally, for years 2015 to 2021, using methods that incorporated local emissions factors, satellite imagery, and other independent approaches to detect where rice production occurred, the number of harvests in each paddy, and annual methane emissions. For the remaining 93 countries that have rice cultivation but were not modeled, an approach was developed using emission factors from Universiti Malaysia Terengganu methodology (Table S1) and The Food and Agriculture Organization (FAO) FAOSTAT reported country-level rice paddy area harvested. This was done to produce a comprehensive global rice emissions dataset that employs rice emission factors that are more reflective of rice cultivation conditions within a country or region.

2. Materials and Methods

The following datasets were used to estimate rice cultivation emissions for the non-modeled 93 countries.

2.1 Datasets

Seasonally integrated methane emission factors (EF) from different countries and regions from Table S1. These emission factors reflect regional and national differences in rice emissions, collected from published data, taken from Universiti Malaysia Terengganu's methodology. Additionally, to better reflect regional emissions in African countries, we employed a rice EF from Zimbabwe taken from Nyamadzawo *et al.* (2013).

For countries and regions that were beyond the spatial mapping threshold set in this work (see section 2.2.1) the IPCC default arithmetic mean emissions factor (Table 4-11) was applied to those countries, IPCC provides a the default emissions factor of 200 kg CH_4 ha^{-1} $season^{-1}$ (converted from the 20 g CH4 m^{-2} $season^{-1}$). The IPCC mean EF was applied to avoid over-applying the Universiti Malaysia Terengganu EF to countries beyond specific geographies, potentially skewing rice emission estimates.

FAOSTAT reported **country-level rice paddy area harvested** for years 2015 to 2020 and **rice cultivation emissions** for years 2015 to 2019. These datasets were used in two ways. First, to combine Universiti Malaysia Terengganu's EFs to FAOSTAT rice areas, at a country-level, to generate a new set of country-level emissions. Second, to compare FAOSTAT rice emission estimates to the rice emission estimates derived in this work. FAOSTAT covers 136 countries, 23 of which were modeled by Universiti Malaysia Terengganu. Of the remaining 113, 93 countries reported emissions and 20 have no rice data (confirmed zeroes).

2.2 Methods

2.2.1 Spatial mapping of EFs

A spatially mapping technique was applied to match countries to the geographically closest EF employed by Universiti Malaysia Terengganu methodology and Nyamadzawo *et al.* (2013). A distance threshold was set to 1000km (a self-defined threshold choice) to identify the closest EF to apply to a specific country. This approach was considered to provide a more reasonable representation of rice EFs in a region. Figure 14 and Table 3 highlight the total number of countries mapped to specific EFs.

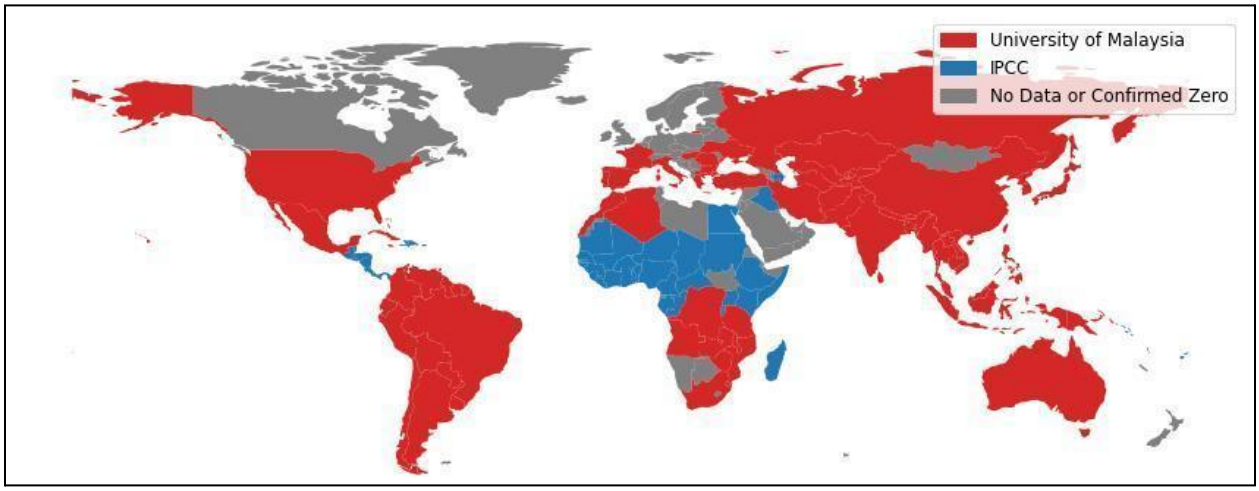

Figure 14 Global map highlighting countries that applied an IPCC rice EF (blue) and countries that used rice EFS from Universiti Malaysia Terengganu's approach (red).

Table 3 Total count of countries that were matched to country specific EF, employed by the Universiti Malaysia Terengganu, or IPCC default EF.

Country-specific or IPCC EF	Total non-modeled countries that used the specific EF	Country-specific or IPCC EF	Total non-modeled countries that used the specific EF
IPCC EF	46	VNM	0
BRA	13	TWN	0
ZWE	9	THA	0
ITA	7	PHL	0
CHN	7	MMR	0
USA	3	KOR	0
IDN	3	KHM	0
ESP	3	JPN	0
MYS	1	BGD	0
IND	1	*Total countries that used a country-specific EF = 47*	

2.2.2 Model

To estimate rice emissions (hereafter, FAO hybrid emissions) for non-modeled countries, the following equation was used, taken from Universiti Malaysia Terengganu methodology:

$$Emission_i = A_i \text{ x } EF_i \text{ (Eq.1)}$$

Where *Emission* is the CH_4 emissions (kg CH_4/ha/season), *A* is the country-level rice paddy area harvested (m^2) from FAOSTAT and *EF* is the emission factor for seasonally rice cultivation (kg CH_4/ha/season) and subscript *i* is for the country. The country EF for seasonal rice cultivation was determined on a distance threshold described in section 2.2.1.

FAOSTAT reported country-level rice paddy area harvested for years 2015 to 2020. To estimate 2021 emissions, 2020 country-level rice paddy area harvested was forwarded-filled to 2021. At the time of this work, FAOSTAT did not publish the 2021 country-level rice paddy area harvested. Once this data is available, the 2021 emissions estimates derived here will be updated accordingly.

3. Result Highlights

Figure 15 compares the annual total emissions between FAOSTAT and FAO hybrid approach. On a global scale, (outside of the Universiti Malaysia Terengganu 23 countries), the FAO hybrid

model produces higher emissions compared to FAOSTAT. The margin between these models is fairly consistent in different years. For each year 2015-2019, the difference between the FAO hybrid model and FAOSTAT's emissions estimates has been between 38.2% and 42.7%, amounting to between 1.35 and 1.88 million tonnes CH_4 difference annually for the countries not modeled by Universiti Malaysia Terengganu. The lower FAOSTAT emissions can be attributed to the overall lower EFs values compared to the 17 country-specific EFs used by Universiti Malaysia Terengganu. For example, the FAO hybrid model applies Brazil's EF of 430.1 kg ha^{-1} $season^{-1}$ to Colombia, Peru, and Ecuador, while FAOSTAT applies a EF value of 20 for each country, which creates an inferred emission factor of 207, 235, and 210 kg ha^{-1} $season^{-1}$ to these countries, respectively.

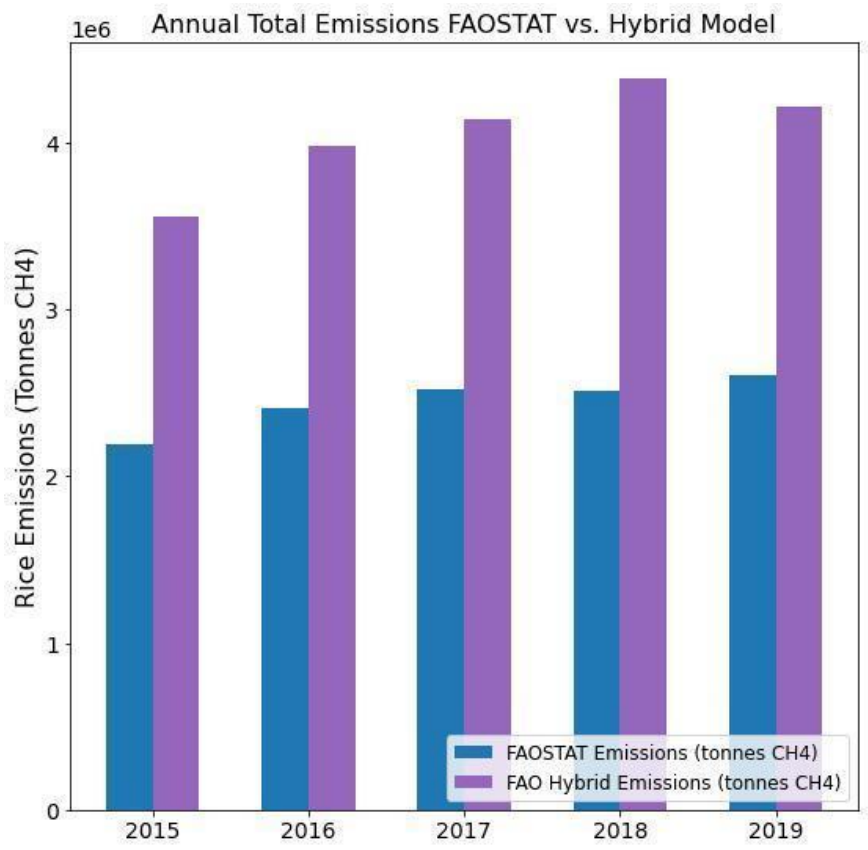

Figure 15 Annual total emissions for 136 countries included in FAOSTAT. Blue bars = FAOSTAT emissions, and purple bars = FAO hybrid emissions (using FAOSTAT reported rice area harvest combined with Universiti Malaysia Terengganu EFs).

Figure 16 highlights country-level total emissions between FAOSTAT and FAO hybrid approach. Countries above the dashed line indicate that the FAO hybrid estimates are higher relative to FAOSTAT emissions. Countries below the dashed line indicate FAOSTAT emission estimates are higher relative to the hybrid approach. Overall, a significant number of countries are above the

dashed line. This is the result of including regional specific rice EFs in the hybrid approach, which results in higher rice methane emissions.

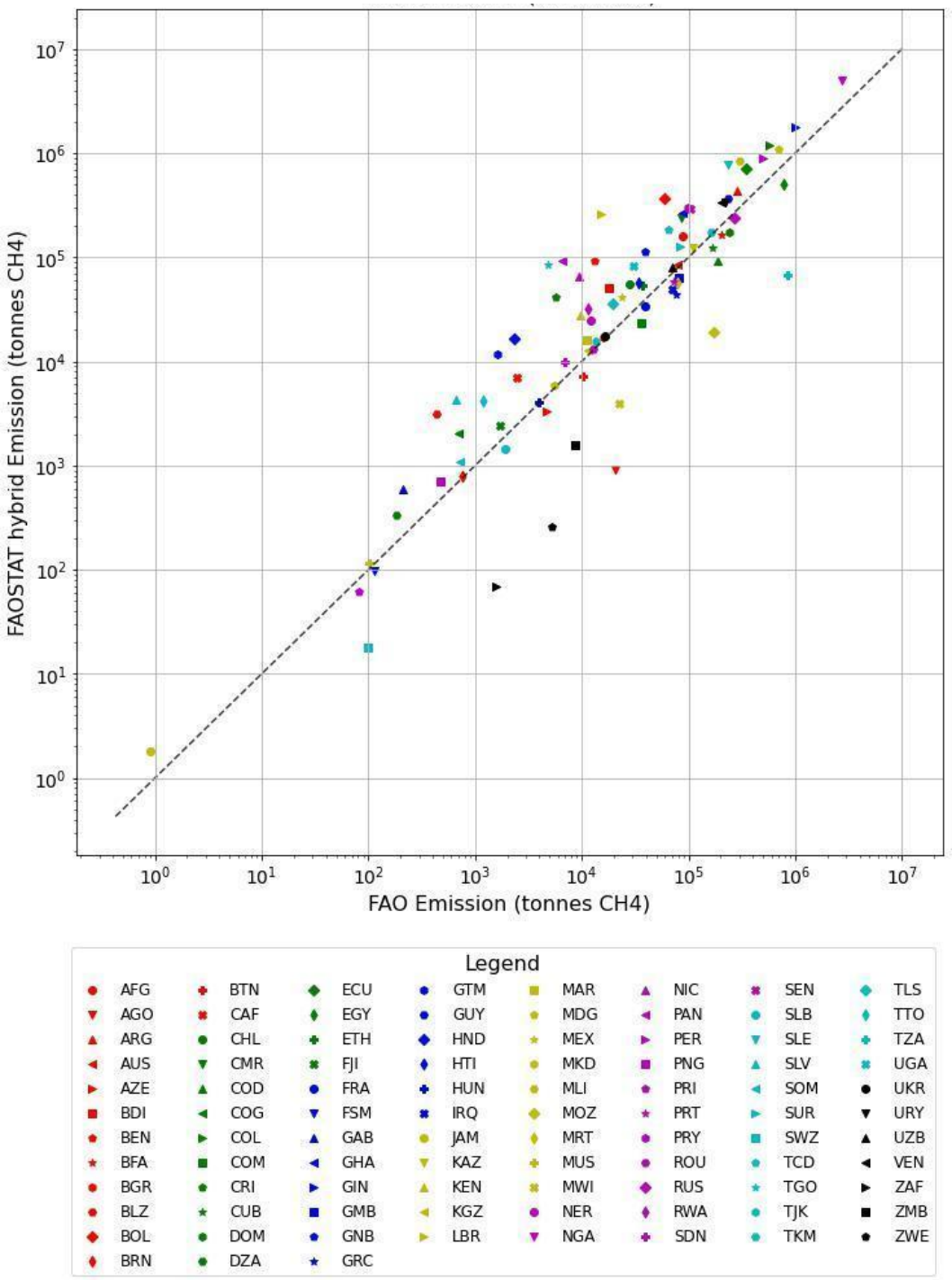

Figure 16 Total emissions for 91 countries from 2015 to 2019 included in FAOSTAT emissions estimates which are not confirmed zeroes. Each unique color and shape correspond to a specific country, indicated by its iso3 code in the legend. X-axis indicates FAOSTAT emissions, whereas

the y-axis indicates FAO hybrid emissions and Universiti Malaysia Terengganu (using FAOSTAT reported rice area harvest combined with Universiti Malaysia Terengganu regional emission factors).

4. Discussion and Conclusion

This approach was created to apply the most recently available rice emission factors to countries outside of the major producing rice countries. In many regions, like South America and southern Africa, we use emission factors from peer-reviewed papers that differ significantly from the default IPCC emission factor. The goal is to provide more up-to-date and reasonable rice emissions in these locations that currently lack their own country-specific emission factor. We prefer these emission factors because they are based on recent research specific to the region and thus reflect the most recent agricultural practices there. In other regions, like western Africa, we employ the default IPCC emission factor, essentially mirroring established practices.

The accuracy of this data could potentially increase as country and regionally specific emissions factors are identified. Western Africa is a region which would particularly benefit from further study, as it contains Nigeria, which is a large rice producer not modeled by Universiti Malaysia Terengganu. Unfortunately, there has not been sufficient study of rice emissions in this region. Lastly, to confirm the approach developed here, identifying *in situ* rice field methane measurements can potentially confirm Climate TRACE emissions estimates and be applied to this approach to better reflect rice cultivation conditions within a country or region.

References

1. Alberto, M.C.R., Wassmann, R., Buresh, R.J., Quilty, J.R., Correa, T.Q., Sandro, J.M., Centeno, C.A.R., 2014. Measuring methane flux from irrigated rice fields by eddy covariance method using open-path gas analyzer. Field Crops Research 160, 12–21. https://doi.org/10.1016/j.fcr.2014.02.008
2. Bhatia, A., Pathak, H., Jain, N., Singh, P.K., Singh, A.K., 2005. Global warming potential of manure amended soils under rice-wheat system in the Indo-Gangetic plains. Atmospheric Environment 39, 6976–6984. https://doi.org/10.1016/j.atmosenv.2005.07.052
3. Camargo, E.S., Pedroso, G.M., Minamikawa, K., Shiratori, Y., Bayer, C., 2018. Intercontinental comparison of greenhouse gas emissions from irrigated rice fields under feasible water management practices: Brazil and Japan. Soil Science and Plant Nutrition 64, 59–67. https://doi.org/10.1080/00380768.2017.1415660
4. Carlson, K.M., Gerber, J.S., Mueller, N.D., Herrero, M., MacDonald, G.K., Brauman, K.A., Havlik, P., O'Connell, C.S., Johnson, J.A., Saatchi, S., West, P.C., 2017. Greenhouse gas emissions intensity of global croplands. Nature Climate Change 7, 63–68. https://doi.org/10.1038/nclimate3158

5. Chang, S.Y.H., 2001. Methane emission from paddy fields in Taiwan 157–165.
6. Della Lunga, D., Brye, K.R., Slayden, J.M., Henry, C.G., Wood, L.S., 2021. Relationships among soil factors and greenhouse gas emissions from furrow-irrigated Rice in the mid-southern, USA. Geoderma Regional 24, e00365. https://doi.org/10.1016/j.geodrs.2021.e00365
7. Dong, J., Xiao, X., 2016. Evolution of regional to global paddy rice mapping methods: A review. ISPRS Journal of Photogrammetry and Remote Sensing 119, 214–227. https://doi.org/https://doi.org/10.1016/j.isprsjprs.2016.05.010
8. Fatchurrachman, Rudiyanto, Soh, N.C., Shah, R.M., Giap, S.G.E., Setiawan, B.I., Minasny, B., 2022. High-Resolution Mapping of Paddy Rice Extent and Growth Stages across Peninsular Malaysia Using a Fusion of Sentinel-1 and 2 Time Series Data in Google Earth Engine. Remote Sensing 14. https://doi.org/10.3390/rs14081875
9. Fazli, P., Man, H.C., 2014. Comparison of Methane Emission from Conventional and Modified Paddy Cultivation in Malaysia. Agriculture and Agricultural Science Procedia 2, 272–279. https://doi.org/10.1016/j.aaspro.2014.11.039
10. Frolking, S., Xiao, X., Zhuang, Y., William Salas, Li, C., 1999. Agricultural land-use in China: a comparison of area estimates from ground-based census and satellite-borne remote sensing . Global Ecology and Biogeography 8, 407–416.
11. Fung, I., John, J., Lerner, J., Matthews, E., Prather, M., Steele, L.P., Fraser, P.J., 1991. Three-dimensional model synthesis of the global methane cycle. Journal of Geophysical Research: Atmospheres 96, 13033–13065. https://doi.org/https://doi.org/10.1029/91JD01247
12. Gale, F., 2013. Growth and evolution in China's agricultural support policies. United States Department of Agriculture Economic Research Service, ERR-153. https://www.ers.usda.gov/webdocs/publications/45115/39368_err153.pdf?v=0
13. Gutierrez, J., Kim, S.Y., Kim, P.J., 2013. Effect of rice cultivar on CH4 emissions and productivity in Korean paddy soil. Field Crops Research 146, 16–24. https://doi.org/10.1016/j.fcr.2013.03.003
14. Hatala, J.A., Detto, M., Sonnentag, O., Deverel, S.J., Verfaillie, J., Baldocchi, D.D., 2012. Greenhouse gas (CO_2, CH_4, H_2O) fluxes from drained and flooded agricultural peatlands in the Sacramento-San Joaquin Delta. Agriculture, Ecosystems and Environment 150, 1–18. https://doi.org/10.1016/j.agee.2012.01.009
15. Humphreys, J., Brye, K.R., Rector, C., Gbur, E.E., 2019. Methane emissions from rice across a soil organic matter gradient in Alfisols of Arkansas, USA. Geoderma Regional 16, e00200. https://doi.org/10.1016/j.geodrs.2018.e00200
16. IPCC, 1997. Revised 1996 IPCC Guidelines for National Greenhouse Gas Inventories. Paris.
17. Islam, S.M.M., Gaihre, Y.K., Islam, M.R., Akter, M., Al Mahmud, A., Singh, U., Sander, B.O., 2020. Effects of water management on greenhouse gas emissions from farmers' rice fields in Bangladesh. Science of the Total Environment 734. https://doi.org/10.1016/j.scitotenv.2020.139382

18. Karki, S., Adviento-Borbe, M.A.A., Massey, J.H., Reba, M.L., 2021. Assessing seasonal methane and nitrous oxide emissions from furrow-irrigated rice with cover crops. Agriculture (Switzerland) 11, 1–15. https://doi.org/10.3390/agriculture11030261
19. Kritee, K., Nair, D., Zavala-Araiza, D., Proville, J., Rudek, J., Adhya, T.K., Loecke, T., Esteves, T., Balireddygari, S., Dava, O., Ram, K., Abhilash, S.R., Madasamy, M., Dokka, R. V., Anandaraj, D., Athiyaman, D., Reddy, M., Ahuja, R., Hamburg, S.P., 2018. High nitrous oxide fluxes from rice indicate the need to manage water for both long- and short-term climate impacts. Proc Natl Acad Sci U S A 115, 9720–9725. https://doi.org/10.1073/pnas.1809276115
20. Kuenzer, C., Knauer, K., 2013. Remote sensing of rice crop areas. International Journal of Remote Sensing 34, 2101–2139. https://doi.org/10.1080/01431161.2012.738946
21. Lagomarsino, A., Agnelli, A.E., Linquist, B., Adviento-Borbe, M.A., Agnelli, A., Gavina, G., Ravaglia, S., Ferrara, R.M., 2016. Alternate Wetting and Drying of Rice Reduced CH4 Emissions but Triggered N2O Peaks in a Clayey Soil of Central Italy. Pedosphere 26, 533–548. https://doi.org/10.1016/S1002-0160(15)60063-7
22. Li, C., Qiu, J., Frolking, S., Xiao, X., Salas, W., Moore III, B., Boles, S., Huang, Y., Sass, R., 2002. Reduced methane emissions from large-scale changes in water management of China's rice paddies during 1980–2000. Geophysical Research Letters 29, 33–34. https://doi.org/https://doi.org/10.1029/2002GL015370
23. Lim, J.Y., Cho, S.R., Kim, G.W., Kim, P.J., Jeong, S.T., 2021. Uncertainty of methane emissions coming from the physical volume of plant biomass inside the closed chamber was negligible during cropping period. PLoS ONE 16, 1–14. https://doi.org/10.1371/journal.pone.0256796
24. Maneepitak, S., Ullah, H., Datta, A., Shrestha, R.P., Shrestha, S., Kachenchart, B., 2019. Effects of water and rice straw management practices on water savings and greenhouse gas emissions from a double-rice paddy field in the Central Plain of Thailand. European Journal of Agronomy 107, 18–29. https://doi.org/10.1016/j.eja.2019.04.002
25. Martínez-Eixarch, M., Alcaraz, C., Viñas, M., Noguerol, J., Aranda, X., Prenafeta-Boldú, F.X., Català-Forner, M., Fennessy, M.S., Ibáñez, C., 2021. The main drivers of methane emissions differ in the growing and flooded fallow seasons in Mediterranean rice fields. Plant and Soil 460, 211–227. https://doi.org/10.1007/s11104-020-04809-5
26. Mazza, G., Agnelli, A.E., Orasen, G., Gennaro, M., Valè, G., Lagomarsino, A., 2016. Reduction of Global Warming Potential from rice under alternate wetting and drying practice in a sandy soil of northern Italy. Italian Journal of Agrometeorology 21, 35–44. https://doi.org/10.19199/2016.2.2038-5625.035
27. Meijide, A., Gruening, C., Goded, I., Seufert, G., Cescatti, A., 2017. Water management reduces greenhouse gas emissions in a Mediterranean rice paddy field. Agriculture, Ecosystems and Environment 238, 168–178. https://doi.org/10.1016/j.agee.2016.08.017

28. Moreno-García, B., Guillén, M., Quílez, D., 2020. Greenhouse gas emissions as affected by fertilization type (Pig Slurry vs. Mineral) and soil management in mediterranean rice systems. Agronomy 10. https://doi.org/10.3390/agronomy10040493
29. Nyamadzawo, G., Wuta, M., Chirinda, N., Mujuru, L. and Smith, J.L., 2013. Greenhouse gas emissions from intermittently flooded (dambo) rice under different tillage practices in Chiota smallholder farming area of Zimbabwe. *Atmospheric and Climate Sciences*, *2013*
30. Oo, A.Z., Sudo, S., Inubushi, K., Mano, M., Yamamoto, A., Ono, K., Osawa, T., Hayashida, S., Patra, P.K., Terao, Y., Elayakumar, P., Vanitha, K., Umamageswari, C., Jothimani, P., Ravi, V., 2018. Methane and nitrous oxide emissions from conventional and modified rice cultivation systems in South India. Agriculture, Ecosystems and Environment 252, 148–158. https://doi.org/10.1016/j.agee.2017.10.014
31. Portmann, F.T., Siebert, S., Döll, P., 2010. MIRCA2000—Global monthly irrigated and rainfed crop areas around the year 2000: A new high-resolution data set for agricultural and hydrological modeling. Global Biogeochemical Cycles 24. https://doi.org/https://doi.org/10.1029/2008GB003435
32. Rudiyanto, Minasny, B., Shah, R.M., Che Soh, N., Arif, C., Indra Setiawan, B., 2019. Automated Near-Real-Time Mapping and Monitoring of Rice Extent, Cropping Patterns, and Growth Stages in Southeast Asia Using Sentinel-1 Time Series on a Google Earth Engine Platform. Remote Sensing 11. https://doi.org/10.3390/rs11141666
33. Sander, B.O., Samson, M., Buresh, R.J., 2014. Methane and nitrous oxide emissions from flooded rice fields as affected by water and straw management between rice crops. Geoderma 235–236, 355–362. https://doi.org/10.1016/j.geoderma.2014.07.020
34. Saunois, M., Bousquet, P., Poulter, B., Peregon, A., Ciais, P., Canadell, J.G., Dlugokencky, E.J., Etiope, G., Bastviken, D., Houweling, S., Janssens-Maenhout, G., Tubiello, F.N., Castaldi, S., Jackson, R.B., Alexe, M., Arora, V.K., Beerling, D.J., Bergamaschi, P., Blake, D.R., Brailsford, G., Brovkin, V., Bruhwiler, L., Crevoisier, C., Crill, P., Covey, K., Curry, C., Frankenberg, C., Gedney, N., Höglund-Isaksson, L., Ishizawa, M., Ito, A., Joos, F., Kim, H.-S., Kleinen, T., Krummel, P., Lamarque, J.-F., Langenfelds, R., Locatelli, R., Machida, T., Maksyutov, S., McDonald, K.C., Marshall, J., Melton, J.R., Morino, I., Naik, V., O'Doherty, S., Parmentier, F.-J.W., Patra, P.K., Peng, C., Peng, S., Peters, G.P., Pison, I., Prigent, C., Prinn, R., Ramonet, M., Riley, W.J., Saito, M., Santini, M., Schroeder, R., Simpson, I.J., Spahni, R., Steele, P., Takizawa, A., Thornton, B.F., Tian, H., Tohjima, Y., Viovy, N., Voulgarakis, A., van Weele, M., van der Werf, G.R., Weiss, R., Wiedinmyer, C., Wilton, D.J., Wiltshire, A., Worthy, D., Wunch, D., Xu, X., Yoshida, Y., Zhang, B., Zhang, Z., Zhu, Q., 2016. The global methane budget 2000--2012. Earth System Science Data 8, 697–751. https://doi.org/10.5194/essd-8-697-2016
35. Saunois, M., Stavert, A.R., Poulter, B., Bousquet, P., Canadell, J.G., Jackson, R.B., Raymond, P.A., Dlugokencky, E.J., Houweling, S., Patra, P.K., Ciais, P., Arora, V.K., Bastviken, D., Bergamaschi, P., Blake, D.R., Brailsford, G., Bruhwiler, L., Carlson, K.M., Carrol, M., Castaldi, S., Chandra, N., Crevoisier, C., Crill, P.M., Covey, K., Curry, C.L.,

Etiope, G., Frankenberg, C., Gedney, N., Hegglin, M.I., Höglund-Isaksson, L., Hugelius, G., Ishizawa, M., Ito, A., Janssens-Maenhout, G., Jensen, K.M., Joos, F., Kleinen, T., Krummel, P.B., Langenfelds, R.L., Laruelle, G.G., Liu, L., Machida, T., Maksyutov, S., McDonald, K.C., McNorton, J., Miller, P.A., Melton, J.R., Morino, I., Müller, J., Murguia-Flores, F., Naik, V., Niwa, Y., Noce, S., O'Doherty, S., Parker, R.J., Peng, C., Peng, S., Peters, G.P., Prigent, C., Prinn, R., Ramonet, M., Regnier, P., Riley, W.J., Rosentreter, J.A., Segers, A., Simpson, I.J., Shi, H., Smith, S.J., Steele, L.P., Thornton, B.F., Tian, H., Tohjima, Y., Tubiello, F.N., Tsuruta, A., Viovy, N., Voulgarakis, A., Weber, T.S., van Weele, M., van der Werf, G.R., Weiss, R.F., Worthy, D., Wunch, D., Yin, Y., Yoshida, Y., Zhang, W., Zhang, Z., Zhao, Y., Zheng, B., Zhu, Q., Zhu, Q., Zhuang, Q., 2020. The Global Methane Budget 2000--2017. Earth System Science Data 12, 1561–1623. https://doi.org/10.5194/essd-12-1561-2020

36. Seto, K.C., Kaufmann, R.K., Woodcock, C.E., 2000. Landsat reveals China's farmland reserves, but they're vanishing fast. Nature 406, 121. https://doi.org/10.1038/35018267
37. Setyanto, P., Pramono, A., Adriany, T.A., Susilawati, H.L., Tokida, T., Padre, A.T., Minamikawa, K., 2018. Alternate wetting and drying reduces methane emission from a rice paddy in Central Java, Indonesia without yield loss. Soil Science and Plant Nutrition 64, 23–30. https://doi.org/10.1080/00380768.2017.1409600
38. Sibayan, E.B., Samoy-Pascual, K., Grospe, F.S., Casil, M.E.D., Tokida, T., Padre, A.T., Minamikawa, K., 2018. Effects of alternate wetting and drying technique on greenhouse gas emissions from irrigated rice paddy in Central Luzon, Philippines. Soil Science and Plant Nutrition 64, 39–46. https://doi.org/10.1080/00380768.2017.1401906
39. Tian, H., Yang, Q., Najjar, R.G., Ren, W., Friedrichs, M.A.M., Hopkinson, C.S., Pan, S., 2015. Anthropogenic and climatic influences on carbon fluxes from eastern North America to the Atlantic Ocean: A process-based modeling study. Journal of Geophysical Research: Biogeosciences 120, 757–772. https://doi.org/https://doi.org/10.1002/2014JG002760
40. Toma, Y., Sari, N.N., Akamatsu, K., Oomori, S., Nagata, O., Nishimura, S., Purwanto, B.H., Ueno, H., 2019. Effects of green manure application and prolonging mid-season drainage on greenhouse gas emission from paddy fields in Ehime, Southwestern Japan. Agriculture (Switzerland) 9, 1–17. https://doi.org/10.3390/agriculture9020029
41. Vibol, S., Towprayoon, S., 2010. Estimation of methane and nitrous oxide emissions from rice field with rice straw management in Cambodia. Environmental Monitoring and Assessment 161, 301–313. https://doi.org/10.1007/s10661-009-0747-6
42. Vo, T.B.T., Wassmann, R., Mai, V.T., Vu, D.Q., Bui, T.P.L., Vu, T.H., Dinh, Q.H., Yen, B.T., Asch, F., Sander, B.O., 2020. Methane emission factors from vietnamese rice production: Pooling data of 36 field sites for meta-analysis. Climate 8. https://doi.org/10.3390/CLI8060074
43. Wang, Z., Zhang, X., Liu, L., Wang, S., Zhao, L., Wu, X., Zhang, W., Huang, X., 2021. Estimates of methane emissions from Chinese rice fields using the DNDC model.

Agricultural and Forest Meteorology 303, 108368. https://doi.org/10.1016/j.agrformet.2021.108368

44. Win, E.P., Win, K.K., Bellingrath-Kimura, S.D., Oo, A.Z., 2020. Greenhouse gas emissions, grain yield and water productivity: a paddy rice field case study based in Myanmar. Greenhouse Gases: Science and Technology 10, 884–897. https://doi.org/10.1002/ghg.2011
45. Yamashita, K., 2009. The pros and cons of Japan's rice acreage-reduction policy. The Tokyo Foundation for Policy Research. https://www.tkfd.or.jp/en/research/detail.php?id=86.
46. Yan, X., Akiyama, H., Yagi, K., Akimoto, H., 2009a. Global estimations of the inventory and mitigation potential of methane emissions from rice cultivation conducted using the 2006 Intergovernmental Panel on Climate Change Guidelines. Global Biogeochemical Cycles 23. https://doi.org/https://doi.org/10.1029/2008GB003299
47. Yan, X., Akiyama, H., Yagi, K., Akimoto, H., 2009b. Global estimations of the inventory and mitigation potential of methane emissions from rice cultivation conducted using the 2006 Intergovernmental Panel on Climate Change Guidelines. Global Biogeochemical Cycles 23. https://doi.org/https://doi.org/10.1029/2008GB003299
48. Zhang, B., Tian, H., Ren, W., Tao, B., Lu, C., Yang, J., Banger, K., Pan, S., 2016. Methane emissions from global rice fields: Magnitude, spatiotemporal patterns, and environmental controls. Global Biogeochemical Cycles 30, 1246–1263. https://doi.org/https://doi.org/10.1002/2016GB005381
49. Zhang, G., Xiao, X., Dong, J., Xin, F., Zhang, Y., Qin, Y., Doughty, R.B., Moore, B., 2020. Fingerprint of rice paddies in spatial–temporal dynamics of atmospheric methane concentration in monsoon Asia. Nature Communications 11, 554. https://doi.org/10.1038/s41467-019-14155-5
50. Zschornack, T., da Rosa, C.M., dos Reis, C.E.S., Pedroso, G.M., Camargo, E.S., Dossantos, D.C., Boeni, M., Bayer, C., 2018. Soil CH4 and N2O emissions from rice paddy fields in southern Brazil as affected by crop management levels: A three-year field study. Revista Brasileira de Ciencia do Solo 42, 1–14. https://doi.org/10.1590/18069657rbcs20170306